Geochimica et Cosmochimica Acta, Vol. 68, No. 23, pp. 4971–4992, 2004

0016-7037/04 $30.00 + .00

doi:10.1016/j.gca.2004.06.008

Timescales determining the degree of kinetic isotope fractionation by evaporation and condensation

FRANK M. RICHTER*

Department of the Geophysical Sciences, University of Chicago, Chicago, IL 60637, USA, and Department of Geology, The Field Museum, Chicago, IL 60605, USA

(*Received December* 12, 2003; *accepted in revised form June* 4, 2004)

Abstract—A first order characteristic of the relative abundance of the elements in solar system materials ranging in size from inclusions in primitive meteorites to planetary sized objects such as the Earth and the Moon is that they are very much like that of the Sun for the more refractory elements but systematically depleted to varying degrees in the more volatile elements. This is taken as evidence that evaporation and and/or condensation were important processes in determining the distinctive chemical properties of solar system materials. In some instances there is also isotopic evidence suggesting evaporation in that certain materials are found enriched in the heavy isotopes of their more volatile elements. Here model calculations are used to explore how the relative rates of various key processes determine the relationship between elemental and isotopic fractionation during partial evaporation and partial condensation. The natural measure of time for the systems considered here is the evaporation or condensation timescale defined as the time it would take under the prevailing conditions for evaporation or condensation to completely transfer the element of interest between the two phases of the system. The other timescales considered involve the rate of change of temperature, the rate at which gas is removed from further interaction with the condensed phase, and the rates of diffusion in the condensed and gas phases. The results show that a key determinant of whether or not elemental fractionations have associated isotopic effects is the ratio of the partial pressure of a volatile element (P_i) to its saturation vapor pressure ($P_{i,sat}$) over the condensed phase. Systems in which the rate of temperature change or of gas removal are slow compared to the evaporation or condensation timescale will be in the limit $P_i \sim P_{i,sat}$ and thus will have little or no isotopic fractionation because at the high temperatures considered here there is negligible equilibrium fractionation of isotopes. If on the other hand the temperature changes are relatively fast, then $P_i \neq P_{i,sat}$ and there will be both elemental and isotopic fractionation during partial evaporation or partial condensation. Rapid removal of evolved gas results in $P_i \ll P_{i,sat}$ which will produce isotopically heavy evaporation residues. Diffusion-limited regimes, where transports within a phase are not sufficiently fast to maintain chemical and or isotopic homogeneity, will typically produce less isotopic fractionation than had the phases remained well mixed. The model results are used to suggest a likely explanation for the heavy silicon and magnesium isotopic composition of Type B CAIs (as due to rapid partial melting and subsequent cooling at rates of a few °C per hour), for the uniformity of the potassium isotopic composition of chondrules despite large differences in potassium depletions (as due to volatilization of potassium by reheating in regions of large but variable chondrules per unit volume), and that the remarkable uniformity of the potassium isotopic composition of solar system materials is not a measure of the relative importance of evaporation and condensation but rather due to the solar nebula having evolved sufficiently slowly that materials did not significantly depart from chemical equilibrium.

1. INTRODUCTION

The relative abundances of the elements in many types of meteorites, as well as the estimated bulk composition of planetary-scale bodies in the inner solar system, are very much like that of the Sun for the more refractory elements but systematically depleted to varying degrees in the more volatile elements (Wänke and Dreibus, 1988; Taylor, 1992; Palme and Boynton, 1993; McDonough and Sun, 1995). These volatility-related elemental depletions of planetary and meteoritic materials are evidence that partial condensation and/or evaporation were important and pervasive processes in establishing the chemical distinctiveness of solar system materials.

Evidence for evaporation in the early solar system comes from coarse-grained Type B Ca-Al-rich inclusions (CAIs) in carbonaceous chondrites that have correlated enrichments in the heavy isotopes of silicon and magnesium (Clayton et al., 1988) very similar to what has been measured in laboratory produced evaporation residues (see fig. 2 in Davis et al., 1990). The Type B CAIs have igneous textures indicating that they were once partially molten for at least several hours (Stolper and Paque, 1986), which when combined with the evaporation kinetics of silicon and magnesium from Type B CAI-like liquids in a low pressure hydrogen-dominated gas (Richter et al., 2002b) leads to the conclusion that they should have suffered significant evaporative loss of these elements while partially molten. The Type B CAIs provide a relatively uncontroversial example of how isotopic fractionations of the more volatile elements are used as a fingerprint of elemental fractionation by evaporation. Chondrules, which are a much more abundant type of inclusion than the CAIs, also often have textures suggesting reheating and high degrees of partial melt-

* Author to whom correspondence should be addressed, at University of Chicago, Department of the Geophysical Sciences, 5734 South Ellis Avenue, Chicago, IL 60637, USA (richter@geosci.uchicago.edu).

ing (Lofgren and Lanier, 1990; Radomsky and Hewins, 1990), however no significant isotopic fractionation of magnesium (Galy et al., 2000) or of the even more volatile elements potassium (Alexander et al., 2000) and iron (Alexander and Wang, 2001) has been found. Galy et al. (2000) attributed the lack of significant magnesium isotopic fractionation to there having been a high total gas pressure (presumably hydrogen) during the reheating of the chondrules. The lack of measurable isotopic fractionation of potassium isotopes was interpreted by Alexander et al. (2000) as indicating that the high temperature event that melted the chondrules evaporated enough potassium to produce a sufficiently high potassium-vapor pressure for gas-chondrule isotopic exchange to be complete on the timescales of chondrule formation. Alexander and Wang (2001) argued that the lack of iron isotopic fractionation could have been due to either very little iron having evaporated because of low hydrogen pressure or by a process of gas-chondrule isotopic exchange similar to what had been invoked for potassium. In the following sections, calculations will be used to explore the role of pressure as it affects isotope fractionation associated with partial evaporation or partial condensation. The models will define what, in the present context, represents high vs. low pressure, and will show how the relative rates of various important processes determine the pressure. The results will allow for a more detailed discussion of the conditions that could have resulted in the Type B CAIs becoming enriched in the heavy isotopes of silicon and magnesium while chondrules, which one expects will have lost significant iron and potassium by evaporation while partially molten, have no significant fractionation of iron and potassium isotopes.

The use of isotopic systematics to constrain the relative importance of evaporation and condensation in determining the bulk composition of planetary size objects including the Moon is becoming quite controversial (see, for example, the recent exchange between Young, 2000, and Humayun, 2001). When considering the relative roles of condensation and evaporation, one should keep in mind that "condensation models" of the sort pioneered by Larimer and Grossman (e.g., Larimer, 1967; Grossman, 1972; and for a more recent version see Ebel and Grossman, 2000) while providing an important framework for discussing the chemical properties of certain primitive solar system materials do not imply that partial condensation was the operative process. These models by assuming that the system is in thermodynamic equilibrium are independent of the path by which the system arrived at any particular state, and thus do not distinguish between partial condensation and partial evaporation. Diagnostic data for making such a distinction will only arise in systems that evolved significantly out of equilibrium. Hinton et al. (1987, 1988) and later Humayun and Clayton (1995) recognized that the isotopic composition of the moderately volatile element potassium might provide diagnostic data with which to distinguish between partial evaporation and partial condensation as the primary cause of the variable volatile element depletion of planetary and meteoritic materials. The structure of the argument as given in Humayun and Clayton (1995) is as follows. The relative depletion of potassium in a broad range of solar system materials can be determined from the K/La ratio because both these elements are lithophile and thus not expected to be significantly fractionated by igneous processes, but because lanthanum is much more refractory than potassium, it can be reasonably assumed that lanthanum will be fully condensed (or not significantly evaporated) in materials containing potassium. Thus, differences in K/La should reflect volatility related depletions of potassium, and by this measure, potassium depletions relative to C1 chondrites span almost two orders of magnitude (e.g., the Earth being depleted by a factor of $\sim$5, the Moon by $\sim$50). Humayun and Clayton (1995) then argued that "the process of partial evaporation can be distinguished from incomplete condensation by the production in the former of large mass-dependent isotopic fractionation (Rayleigh distillation) in elements that otherwise lack isotopic variations in nature" whereas "such effects are not produced during condensation, as long as the gas is well mixed (i.e., no diffusive or gravitational separation of isotopes has taken place), since the rate of uptake of the isotopes at the surface of a condensed phase is controlled by thermodynamic factors, and not by the rate at which gas is supplied to the surface." With this in mind, they measured the potassium isotopic composition of a variety of solar system materials with different K/La and found no significant variation in the $^{41}K/^{39}K$ ratio at the level of their typical precision of $\sim$1‰. Based on their claim that partial evaporation always produces isotopic fractionation they interpreted the lack of measurable isotopic fractionation of the potassium isotopes as "placing stringent limits of $\leq$2% on the quantity of potassium that could have been lost by partial volatilization."

I will use both experimental data and model calculations based on the generally accepted description of evaporation and condensation derived from the kinetic theory of gases (see Hirth and Pound, 1963) to dispute the claim that evaporation always produces mass-dependent isotope fractionation and that no isotopic fractionation is produced during condensation from a well-mixed gas. I will show that there are conditions such that both partial evaporation and partial condensation can produce an isotopically fractionated condensed phase, and I will also show that there are conditions where partial evaporation and partial condensation can fractionate elements by volatility without measurable isotopic fractionation. A key fact to keep in mind is that equilibrium processes can fractionate elements based on their relative volatility whereas equilibrium isotopic fractionations are negligibly small at the high temperatures required to significantly volatilize elements such as magnesium, iron, and potassium from partially molten silicate systems. Thus systems evolving close to equilibrium can fractionate elements by volatility without significant isotopic fractionation. In order for there to be isotopic fractionation during either evaporation or condensation some aspect of the kinetics has to be sufficiently fast or slow to keep the system from maintaining equilibrium. The processes that will be considered in the following sections involve both mass transports between phases (i.e., the rates of evaporation and condensation) and transports within phases (i.e., the rates of advection and diffusion). Model calculations will be used to illustrate how departures from thermodynamic equilibrium depend on the relative rates of these transport processes and also on whether they are fast or slow compared to the rate of change of key environmental variables such as temperature. An important process that will not be included in the present set of models is exchange between solid and liquid phases (i.e., crystallization or resorption of minerals) for the reason that it is not directly

affected by the rates and associated timescales that are the main focus of this paper. Readers interested in the effect of crystallization during evaporation are referred to the recent model calculations by Grossman et al. (2002), although it should be noted that the thermodynamic model used in this effort can predict crystallization temperatures for major minerals that are off by as much as 100°C from what is found in experiments (see Mendybaev et al., 2003).

In the following section the generally accepted theory for evaporation and condensation is reviewed and then used in later sections to develop simple model problems that illustrate the effect of various timescales on the degree of isotopic fractionation associated with elemental fractionation during evaporation and condensation. Much of the modeling and discussion focuses on the isotopic fractionation of magnesium during evaporation and condensation of either a Type B CAI-like composition or forsterite, these being the materials for which the most detailed experimental data on evaporation kinetics and isotopic fractionation are available. The focus on CAI-like compositions and forsterite also derives from their relationship to the equilibrium condensation behavior of elements from a cooling gas of solar composition. The Type B CAI-like composition used for the model calculations (~15 wt% MgO, 40 wt% SiO_2, 20% CaO, 25% Al_2O_3) is similar to condensate compositions once ~5% of the magnesium has condensed, while forsterite takes in the next 90% of the condensable magnesium from the cooling solar composition gas (see Yoneda and Grossman, 1995). It is also worth noting that the equilibrium condensates are predicted to be solids for all reasonable total pressures ($P_{tot} < 10^{-2}$ atm) of the solar composition gas (see Yoneda and Grossman, 1995) and that partially melting Type B CAI-like compositions (Stolper, 1982; Richter et al., 2002a) requires reheating to several 100 K above their condensation temperature.

The emphasis on magnesium should not obscure the fact that the model results are meant to be quite general in that they depend on nondimensional parameters that in principle could have been specified for some other element of interest. Indeed, many of the models discussed here, particularly those focused on evaporation, can be considered simplified versions of the much more detailed and exhaustive models already developed by Ozawa and Nagahara (2001). Model problems that despite their simplicity still capture the essentials of the system being studied do have their virtues in that they often render the results more intuitively understandable. In the present case a key determinant of the relationship between elemental and isotopic fractionation during partial evaporation or partial condensation is the partial pressure of the evaporating species at the surface relative to the saturation vapor pressure. A distinctive feature of the approach adopted here is the emphasis on how the various natural timescales of evaporating and condensing systems determine the relative magnitude of these two pressures.

2. THEORETICAL CONSIDERATIONS

A detailed mathematical formulation of evaporation and condensation was given by Hirth and Pound (1963). For present purposes, I will use a somewhat simplified version applicable to situations such as those considered here where the equilibrium gas species of a given element of interest are dominantly of a single type. The net flux J_i of an element i between a condensed phase and a surrounding gas is given by

$$J_i = \frac{n\gamma_i(P_{i,sat} - P_i)}{\sqrt{2\pi m_i RT}} \quad (1)$$

J_i is the flux of i in moles per unit area per unit time (positive indicating net evaporation), n is the number of atoms of i in the dominant gas species molecule containing i, γ_i is a sticking coefficient, $P_{i,sat}$ and P_i are the saturation vapor pressure and partial pressure of the gas molecule containing i at the surface of the condensed phase, m_i is the molar mass of the gas species molecule containing i, R is the gas constant, and T is the absolute temperature. The simplification of considering only one gas species per element in Eqn. 1 is appropriate for elements such as magnesium and silicon in that the gas in equilibrium with the condensed phases considered here will be dominated by Mg and SiO. The same will be true for the speciation of iron and potassium (as Fe and K) in a gas in equilibrium with a chondrule-like composition. For all these gas species $n = 1$, and thus n will not be explicitly included in any of the equations given below. Eqn. 1 is closely related to the kinetic theory of gases in that the quantity $J_i = P_i/\sqrt{2\pi m_i RT}$ is the rate at which the gas species containing i impinge on the surface. In many cases, only a fraction of the species impinging on the surface actually condense, which is accounted for by the sticking coefficient γ_i (≤ 1). The evaporation flux is assumed proportional to $P_{i,sat}$ based on the requirement that as the system approaches equilibrium, $P_i \rightarrow P_{i,sat}$ and the net flux must tend to zero. The opposite limit, $P_i/P_{i,sat} \rightarrow 0$ will be referred to as the free evaporation or vacuum limit. Laboratory experiments are required in connection with Eqn. 1 because there is no general theory for calculating γ_i. In practice γ_i is determined by requiring that the evaporation flux calculated using Eqn. 1 in the limit $P_i/P_{i,sat} \rightarrow 0$ reproduce the flux measured in vacuum experiments. Eqn. 1 implicitly assumes that the condensation flux and the evaporation flux are limited by the same sticking coefficient regardless of the actual value of $P_i/P_{i,sat}$. Sticking coefficients are sometimes very close to one (for example, Wang et al., 1994 reported $\gamma_{Fe} = 1$ for iron evaporating from liquid FeO; Tsuchiyama et al., 1995 and Tachibana et al., 2001 found a similar result for the evaporation of Fe metal), however for silicon and magnesium evaporating from silicate liquids γ is in the range 0.1–0.01 depending on the temperature at which the evaporation takes place (see fig. 10 in Richter et al., 2002b).

Eqn. 1 can be used to contrast kinetic and equilibrium mechanisms of elemental fractionations by volatility. The ratio of the evaporation flux of two elements indicated by the subscripts *1* and *2* is of the form

$$\frac{J_1}{J_2} = \left(\frac{\gamma_1(P_{1,sat} - P_1)}{\gamma_2(P_{2,sat} - P_2)}\right)\sqrt{\frac{m_2}{m_1}} \quad (2)$$

The role of volatility enters via the saturation vapor pressures, however one should note that the ratio of sticking coefficients, which could be as large (or small) as a factor of 100 (or 0.01), could also have a significant effect on elemental fractionations

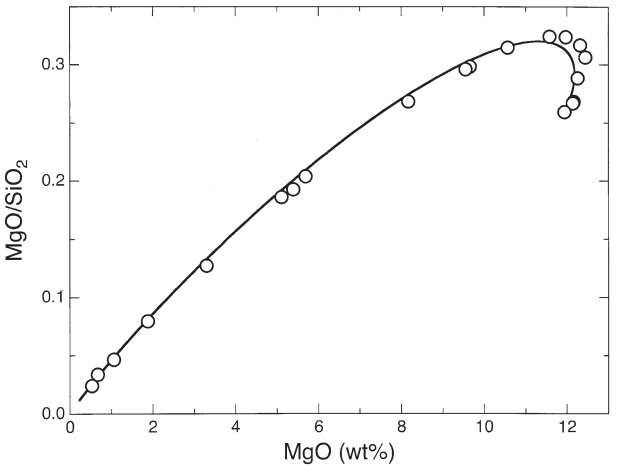

Fig. 1. The Si/Mg ratio as a function of the wt% MgO remaining in vacuum evaporation residues is shown as open circles. These data are from a new set of evaporation residues produced in the University of Chicago vacuum furnace and analyzed for major element composition in the manner described in Richter (2002b). The starting composition was 22.5 wt% CaO, 12.0 wt% MgO, 19.5 wt% Al_2O_3, and 46.0 wt% SiO_2. The continuous curve is Si/Mg ratio as a function of wt% MgO in evaporation residues calculated using Eqn. 2 with $P_{Mg} = 0$, $P_{Si0} = 0$, $\gamma_{Mg} = \gamma_{Si}$, and the saturation vapor pressures of Mg and SiO calculated using the thermodynamic model described in Grossman et al. (2000).

by kinetic processes. The inverse square root of the atomic mass term is generally much less important in terms of fractionating major rock forming elements. If the system is allowed to reach equilibrium, elements can still be fractionated by volatility in that once an element begins to condense the amount of that element in the condensed phase must be such that the partial pressure in the gas equals the saturation vapor pressure. Thus

$$\left(\frac{N_1}{N_2}\right)_{cond} = \frac{N_{1,tot}\left(1 - \frac{P_{1,sat}}{P_{1,max}}\right)}{N_{2,tot}\left(1 - \frac{P_{2,sat}}{P_{2,max}}\right)} \quad (3)$$

where $(N_1/N_2)_{cond}$ is the element ratio in the condensed phase, $N_{1,tot}/N_{2,tot}$ is the ratio of all of element *1* and *2* in the system, and $P_{1,max}$ and $P_{2,max}$ are the pressures corresponding to all of element *1* and *2* being in the gas at the temperature being considered. An important potential difference between elemental fractionation by kinetic (Eqn. 2) and equilibrium processes (Eqn. 3) comes from the possibility that the ratio of the sticking coefficients is significantly different from one. For example, if iron evaporating from a silicate liquid has $\gamma_{Fe} \approx 1$, as it has for iron evaporating from FeO, while for magnesium $\gamma_{Mg} \approx 0.03$, then iron will in effect be ~30 times more volatile relative to magnesium during kinetic evaporation than the more usual measure of their relative volatility based on saturation vapor pressures alone.

The applicability of Eqn. 1 for describing the elemental fractionation by evaporation from a silicate liquid can be tested by comparing the chemical evolution of laboratory-produced residues to that calculated using Eqn. 2. Figure 1 shows the fractionation of the SiO_2 and MgO components of CMAS liquids (molten CaO-MgO-Al_2O_3-SiO_2) that were evaporated to varying degrees in a vacuum furnace ($P \leq 10^{-6}$ Torr) at T = 1800°C. Also shown is a calculated evolution curve based on Eqn. 2 in the limit $P_{i,sat} \gg P_i$ appropriate to the very low pressure conditions of the experiments. The agreement between the experimental data and the calculated evolution shown in Figure 1, and similarly good results given in Richter et al. (2002b), is evidence that Eqn. 1 when used together with Berman's (1983) thermodynamic model for the solution properties of the silicate liquids provides an accurate representation of the free evaporation of volatile components from molten CAI-like compositions.

Eqn. 2 can also be used to calculate the kinetic fractionation of isotopes by partial evaporation. In the case of evaporation of isotopically distinct gas species of mass m_1 and m_2.

$$\frac{J_1}{J_2} = \frac{\gamma_1}{\gamma_2}\left(\frac{P_{1,sat} - P_1}{P_{2,sat} - P_2}\right)\sqrt{\frac{m_2}{m_1}} \quad (4)$$

In the vacuum limit $P_i/P_{i,sat} \ll 1$, this equation becomes

$$\frac{J_1}{J_2} = \frac{\gamma_1 P_{1,sat}}{\gamma_2 P_{2,sat}}\sqrt{\frac{m_2}{m_1}} = \frac{N_1}{N_2}\frac{\gamma_1}{\gamma_2}\sqrt{\frac{m_2}{m_1}} = R_{12}\frac{\gamma_1}{\gamma_2}\sqrt{\frac{m_2}{m_1}} \quad (5)$$

where R_{12} is the atom ratio, N_1/N_2 in the condensed phase. In writing Eqn. 5 it is assumed that $P_{1,sat}/P_{2,sat} = N_1/N_2$, which follows from the ideal mixing properties of isotopes and that all the application considered in this paper involve sufficiently high temperatures (T > 1000 K) that equilibrium fractionations can be neglected. The kinetic isotope fractionation factor α, defined in terms of the isotopic composition of flux relative to the source is then $\alpha = (\gamma_1/\gamma_2)\sqrt{m_2/m_1}$. It is usually assumed that the sticking coefficient for isotopes of the same element are the same, in which case α is simply $\alpha = \sqrt{m_2/m_1}$.

The cumulative effect of the fractionation given by Eqn. 5 is easily calculated if it is further assumed that mass transport processes (e.g., chemical diffusion) are sufficiently fast to maintain the chemical and isotopic homogeneity of the condensed phase. In this case the conservation equation for the isotope i in a volume V with surface area A becomes

$$dN_i = -J_i A \quad (6)$$

where N_i is the atoms of i in V and the flux is now in units of atoms of i per unit area per unit time. With the assumption that $\gamma_1 = \gamma_2$, combining Eqns. 5 and 6 gives

$$\frac{dN_1}{dN_2} = \left(\frac{N_1}{N_2}\right)\sqrt{\frac{m_2}{m_1}} \quad (7)$$

or equivalently

$$\frac{dN_1}{N_1} = \alpha \frac{dN_2}{N_2} \quad (8)$$

with $\alpha = \sqrt{m_2/m_1}$. Eqn. 8 can be integrated from the starting isotopic abundances $N_{1,0}$, $N_{2,0}$ to that at any later time (when the abundances are N_1 and N_2), yielding

$$\ln\left(\frac{N_1}{N_{1,0}}\right) = \alpha \ln\left(\frac{N_2}{N_{2,0}}\right) \quad (9)$$

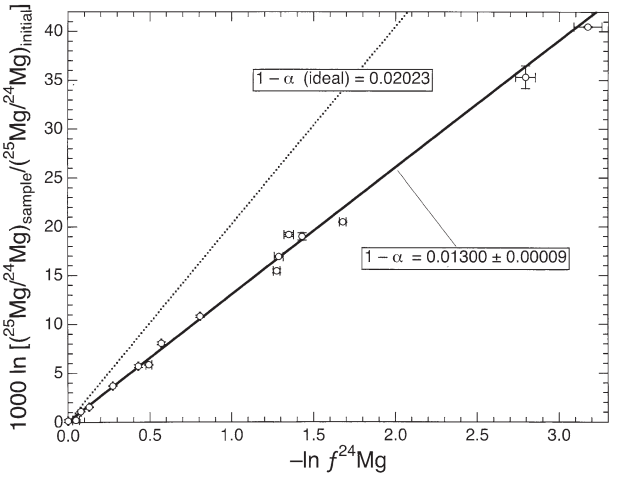

Fig. 2. Open circles show the 1000 × ln (R/R_0) of evaporation residues (where R is the $^{25}Mg/^{24}Mg$ ratio and R_0 is the ratio of the stating material) plotted against $-\ln f^{24}_{Mg}$ where f^{24}_{Mg} is the fraction of ^{24}Mg remaining in the residue. Rayleigh fractionation (Eqn. 11) produces a straight line in this type of a plot with intercept (0,0) and slope 1000 × ($1 - \alpha$). The data are best fit with a value of $\alpha = 0.987$ rather than the expected $\alpha = (24/25)^{1/2} = 0.9798$ (see text). Lines corresponding to these two values for α are shown.

or equivalently

$$\frac{N_1}{N_{1,0}} = \left(\frac{N_2}{N_{2,0}}\right)^{\alpha} \tag{10}$$

Dividing Eqn. 10 by $N_2/N_{0,2}$ and writing the isotope ratios as $R_{12} = N_1/N_2$ and $R_0 = N_{1,0}/N_{2,0}$ results in the familiar Rayleigh fractionation relationship (Rayleigh, 1896)

$$\frac{R_{12}}{R_0} = \left(\frac{N_2}{N_{2,0}}\right)^{\alpha-1} \approx f^{\alpha-1} \tag{11}$$

($N_2/N_{2,0}$) is the fraction of isotope 2 remaining in the condensed phase. A common practice is to use the approximate version of Eqn. 11 written in terms of the fraction f of total element remaining in the residue, which is reasonable for sufficiently small changes in the isotope ratio.

There are a number of laboratory vacuum evaporation experiments (e.g., Davis et al., 1990; Wang et al., 2001; Richter et al., 2002b) that provide data with which to assess the validity of Eqn. 11 for calculating kinetic isotope fractionations during the partial evaporation of silicate liquids. Figure 2 shows some recently obtained high-precision magnesium isotopic data (see Janney et al., 2003 for details) measured on a subset of the evaporation residues that were used to construct Figure 1. The data are plotted as ln (R_{12}/R_0) vs. $-\ln f^{24}_{Mg}$ (f^{24}_{Mg} is the fraction of ^{24}Mg remaining in the residue), which according to Eqn. 11, should be a straight line with slope $1 - \alpha = 0.0202$ for the isotope ratio $^{25}Mg/^{24}Mg$ (i.e., $1 - \sqrt{24/25} = 0.0202$). The data in Figure 2 deviate very little from a straight line implying Rayleigh fractionation with a constant α_{Mg}, however, the value of α_{Mg} derived from the slope of the line ($1 - \alpha_{Mg} = 0.0130$; $\alpha_{Mg} = 0.9870$) is not equal to $\sqrt{24/25}$ (= 0.9798). Similar departures from $\alpha_{Mg} = \sqrt{24/25}$ were found in many earlier experiments (e.g., Richter et al., 2002b: $\alpha_{Mg} = 0.9892$ for a different set of CMAS evaporations in vacuum, and $\alpha_{Mg} = 0.9869$ for CMAS evaporations in 1.87×10^{-4} bars hydrogen; Wang et al., 2001: $\alpha_{Mg} = 0.9843$ for vacuum evaporation of a liquid with solar proportions of the major oxides; Davis et al., 1990: $\alpha_{Mg} = 0.9850$ for vacuum evaporations of liquid forsterite). The issue of whether these differences between the experimentally determined and the theoretically expected value of α_{Mg} are more likely due to imperfections of the experiments or false expectations (i.e., that isotopes of a given element have the same sticking coefficient) will be the subject of a future paper. For present purposes, the important point is that the magnesium isotopic fractionations of CMAS evaporation residues run in the limit $P_i/P_{i,sat} \ll 1$ are consistent with Rayleigh fractionation with constant α. Vacuum evaporations of iron from molten FeO (Wang et al., 1994) and potassium evaporating from a chondrule-like composition in 10^{-5} atm of air (Yu et al., 2003) resulted in kinetic isotope fractionations that follow a Rayleigh law with a value of α corresponding to the inverse square root of the mass of the evaporating isotopes. The calculations discussed in the following sections use values of α corresponding to $\alpha = \sqrt{m_2/m_1}$ even for Mg, where I'm more inclined to believe the experimentally determined value. Given that the purpose of the model calculations is to demonstrate the effect of various timescales on kinetic isotope fractionations rather than pretend to quantitative rigor, the exact choice of α is not important so long as it differs from one.

Another simple but useful limiting case arises when the gas pressure is significantly greater than the saturation vapor pressure (i.e., $P_i \gg P_{i,sat}$). This represents the case of condensation from a highly supersaturated state and the isotopic composition of the uncondensed gas will become increasingly heavy by Rayleigh fractionation as given by an equation analogous to Eqn. 11 with the variables now referring to properties of the gas. The condensate will have a bulk isotopic composition given by

$$\frac{R_{12}}{R_0} = \frac{(1 - f_2^{\alpha})}{(1 - f_2)} \tag{12}$$

where R_{12} the isotopic ratio in the condensate, R_0 is the initial ratio in the gas, and f_2 is the fractional amount of isotope 2 remaining in the gas.

Isotopic fractionations in particular limiting cases of evaporation ($P_{i,sat} \gg P_i$) and condensation ($P_i \gg P_{i,sat}$) are illustrated in Figure 3 for the $^{25}Mg/^{24}Mg$ ratio. In the case of free evaporation, the condensed phase is the source reservoir and the gas, the sink, while for condensation, the gas is the source and the condensed phase the sink. The isotopic composition of each increment added to the sink is (α-1) × 1000‰ lighter than the source, and is also shown. In the following sections a variety of model problems are used to illustrate how various key time scales related to evaporation or condensation determine when evaporating or condensing systems approach the limiting behaviors shown in Figure 3 or how they depart in predictable ways by reducing the isotopic fractionation associate with a given amount of elemental fractionation.

3. EVAPORATION AND CONDENSATION TIMESCALES

The rates of evaporation and condensation define timescales against which all other rates will be measured. Situations in-

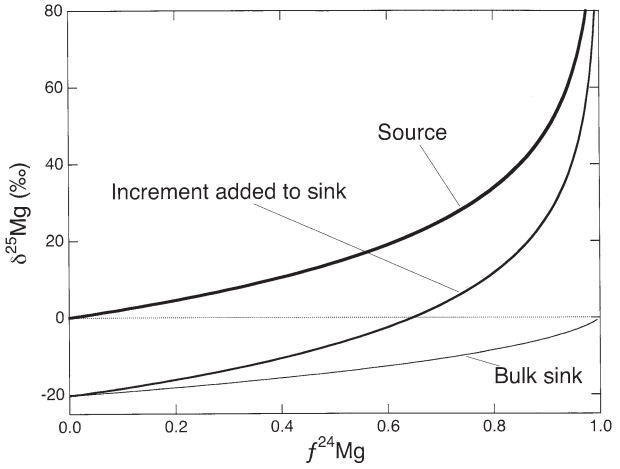

Fig. 3. The three curves plotted in this figure are respectively the magnesium isotopic composition of a Rayleigh fractionating source (condensed phase in the case of evaporation, gas in the case of condensation), the bulk sink (condensed phase in the case of condensation, gas in the case of evaporation), and the instantaneous flux from source to sink plotted as a function of the fraction $f_{^{24}Mg}$ of the original ^{24}Mg remaining in the sink. The isotopic composition of the source was calculated using Eqn. 11, that of the bulk sink using Eqn. 12, and the instantaneous flux is always $1000 \times (1 - \alpha)$ ‰ lighter than the source. A value of $\alpha = \sqrt{24/25} = 0.9798$ was used to calculate the various isotopic compositions. Here and throughout this paper isotopic fractionations relative to the unfractionated magnesium isotopic ratio $(^{25}Mg/^{24}Mg)_0$ are given in ‰ as $\delta^{25}Mg = [(^{25}Mg/^{24}Mg)/(^{25}Mg/^{24}Mg)_0 - 1] \times 1000$.

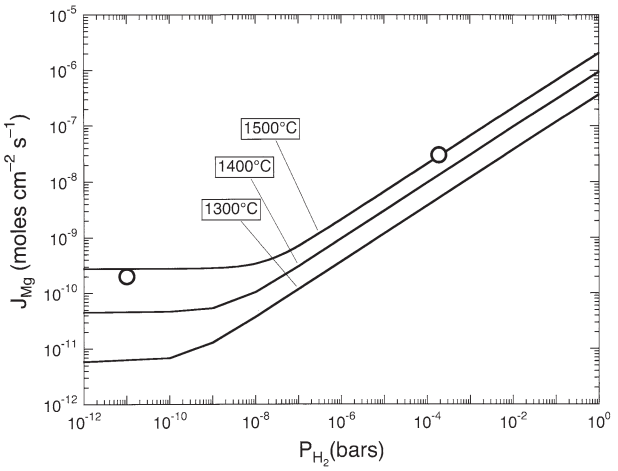

Fig. 4. Free evaporation rate of magnesium as a function of hydrogen pressure for three temperatures. The open circles are based on experimental evaporation rates and the continuous curves are based on parameterizations by Richter et al. (2002b).

volving evaporation are typically much easier to specify in terms of initial conditions (e.g., evaporation of a molten CAI-like droplet of specified size and composition by a specified thermal history). A natural measure of the evaporation timescale, τ_{evap}, is the time it would take for the evaporation flux corresponding to the initial state to exhaust a component of interest in the condensed phase. This timescale is given by

$$\tau_{evap} = \frac{V_c \rho_i}{A J_i} \tag{13}$$

where V_c is the volume of the condensed phase (e.g., cm^3), ρ_i is the molar density of i in the condensed phase (e.g., moles cm^{-3}), A is surface area (e.g., cm^2) and J_i is the flux of i in moles cm^{-2}. $V/A = r/3$ for a sphere of radius r, and $V/A = L$ for a slab of half thickness L evaporating from both surfaces.

A useful limiting estimate of the evaporation timescale is obtained by assuming free evaporation (i.e., $P_i \ll P_{i,sat}$), which by ignoring recondensation will give the shortest possible timescale. The two condensed systems for which there is sufficient kinetic data on evaporation involve forsterite and CMAS liquids. Figure 4 shows how the evaporation rate of magnesium from a Type B CAI-like liquid depends on temperature and hydrogen pressure based on experimental data and parameterizations given in Richter et al. (2002b). Figure 5 shows corresponding estimates for the evaporation timescale for magnesium as a function of temperature and pressure for $r = 0.25$ cm, which is typical for a Type B CAI. Figure 6 gives some examples of the evaporation timescales for solid forsterite as a function of temperature, pressure, and size based on the following representation of the evaporation rate of forsterite in vacuum

$$J_{Fo} = 6.0 \times 10^{-6} e^{\frac{-E}{R}\left(\frac{1}{T} - \frac{1}{T_0}\right)} \tag{14}$$

where R is the gas constant and with an activation energy $E = 630$ kJ mol^{-1} and $T_0 = 2073.15$ K chosen to fit the evaporation kinetic data of Wang et al. (1999). For forsterite evaporating in the hydrogen-dominated regime ($P_{H_2} \geq 10^{-6}$ bars) the flux is calculated from

$$J_{Fo} = 2.3 \times 10^{-8} \sqrt{\frac{P_{H_2}}{P_0}}\, e^{\frac{-E}{R}\left(\frac{1}{T} - \frac{1}{T_0}\right)} \tag{15}$$

where P_{H_2} is the hydrogen pressure in bars. The reference pressure $P_0 = 1.8 \times 10^{-4}$ bars, activation energy $E = 350$ kJ mol^{-1}, and

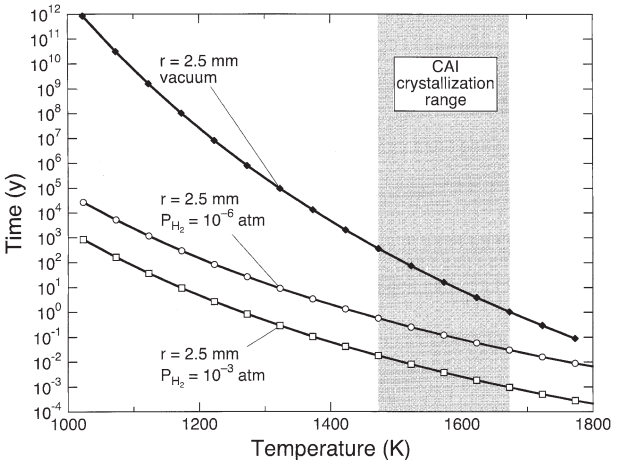

Fig. 5. Evaporation timescales for magnesium from a molten CMAS sphere of radius 0.25 cm as a function of temperature and hydrogen pressure. The shaded area indicates the range of temperatures over which a Type B CAI-like liquid will be partially molten.

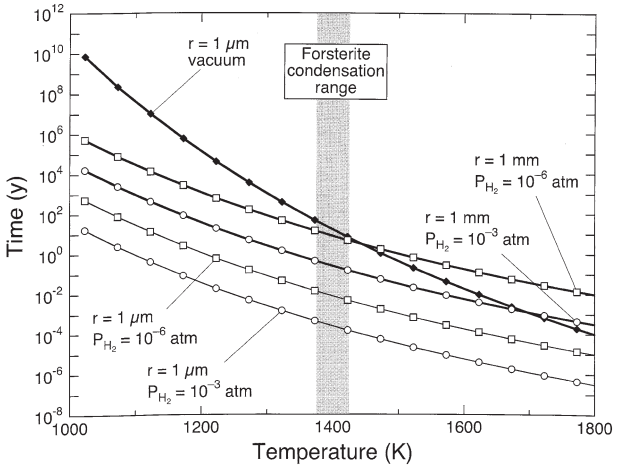

Fig. 6. Evaporation timescales for magnesium from a forsterite sphere of radius 1 mm and 1 μm as a function of temperature and hydrogen pressure. The shaded area indicates range of temperatures over which forsterite condenses from a solar composition gas of total pressure 10^{-3} atm.

reference temperature $T_0 = 1773.15$ K were chosen to fit the kinetic data for forsterite evaporating into hydrogen reported by Kuroda and Hashimoto (2002).

Estimating realistic timescales for condensation is often much less straightforward than for evaporation because of the difficulty in specifying the surface area on which condensation takes place and reasonable degrees of supersaturation. One way to proceed is to introduce a new parameter ϕ such that the degree of supersaturation is given by $P_i = (1 + \phi)P_{i,sat}$, and assume that the system contains M_i moles of the component of interest that will condense into η equal spheres or slabs. In the special case where the species i condenses as part of a one-component condensed phase (e.g., magnesium condensing as forsterite), the radius once all of i has condensed will be

$$r = \left(\frac{\nu_i M_i}{4/3\pi\eta}\right)^{\frac{1}{3}} = \eta^{-\frac{1}{3}} r_{\max} \tag{16}$$

where ν_i is the molar volume of component i and r_{max} is the final radius if all of the M_i moles had condensed into a single sphere. If we consider systems containing the same number of moles of i, the condensation timescale can be defined in relation to the evaporation timescale for a sphere of radius r_{max} by

$$\tau_{cond} = \frac{\eta^{-\frac{1}{3}}\tau_{evap}}{\phi} \tag{17}$$

In the case of condensation onto slabs, η has no affect on the condensation timescale because the total surface to total volume ratio is independent of the number of slabs, and thus η should be set equal to one in Eqn. 17 regardless of the actual number of slabs. Model calculations discussed below will show that the supersaturation parameter ϕ can vary by a large amount depending on whether the rate of condensation is fast or slow compared to the rate of change of environmental parameters such as temperature. Thus, there is no generally appropriate a priori choice for ϕ. This is not a serious limitation, however, because the degree of supersaturation as a function of time will be part of what is solved for in the condensation problems considered below. The experimental data on nucleation of silicate phases from a vapor are still too limited to allow for any a priori estimates of the nucleation density, thus the factor η will be treated as a free parameter. The condensation nuclei density parameter η will not appear explicitly in the model problems when one measures time in units of τ_{cond}, however, the uncertainty in η will of course compromise converting nondimensional time back into dimensional units.

The timescales given by Eqns. 13 and 17 are for various reasons lower bounds on the actual time scales that might be realized in a natural system. The evaporation time scale given by Eqn. 13 is based on the initial surface area, which for a finite body such as a sphere, will decrease to some degree as evaporation proceeds with the effect of increasing the timescale for further evaporation. In situations where the evaporation is not congruent (e.g., evaporation of magnesium from a CMAS liquid), the evaporation time will also tend to be longer than that given by Eqn. 13 because the chemical activity and thus the saturation vapor pressure of the more rapidly evaporating components will typically decrease as evaporation proceeds with the effect of reducing the evaporation rate. The timescale given by Eqn. 13 is also a lower bound because it ignores recondensation. In the case of the condensation, the timescale given by Eqn. 17, being based on the final surface area, could result in a significant underestimate of the condensation time. One should keep in mind that as long as one does not neglect terms in the governing equations on the basis of these estimated timescales, the solutions will be valid regardless of whether or not one has made a reasonable a priori estimate of the timescales. The mismeasure of the timescales will show up by the system evolving very rapidly or very slowly when time is measured in units of the misestimated timescales.

4. ENVIRONMENTAL CHANGE TIMESCALE

In this section model problems will be used to illustrate the consequences of the environmental conditions in a closed system changing rapidly or slowly compared to the characteristic timescales of evaporation and condensation. The measure of whether the environment, specified here in terms of temperature, changes rapidly or slowly is given by the ratio

$$\varepsilon = \frac{\tau_{evap}}{\tau_T} = \frac{\lambda_T V_c \rho_i}{A J_{i,0}} \tag{18}$$

or in the case of condensation by

$$\varepsilon = \frac{\tau_{cond}}{\tau_T} = \frac{\lambda_T V_c \rho_i \eta^{-\frac{1}{3}}}{A J_{i,0}} \tag{19}$$

where τ_T is a timescale for temperature change based on the cooling rate $\lambda_T = -(1/T)dT/dt$ ($\tau_T = \lambda_T^{-1}$) and $J_{i,O}$ is the free evaporation rate at some specified T and P (e.g., from Fig. 4 or equations such as Eqns. 14 and 15). The nucleation density parameter η is set equal to one if Eqn. 19 is used for a slablike geometry.

The model problems considered in this section involve the conservation equations for a closed system (except for heat) along with statements specifying thermodynamic properties.

Assuming a spherical condensate of uniform composition, the governing equations can be written as

$$\frac{dM_i}{dt} = -4\pi r^2 \eta J_i \tag{20}$$

$$J_i = \frac{\gamma_i (P_{i,sat} - P_i)}{\sqrt{2\pi m_i RT}} \tag{21}$$

$$P_{i,sat} = fn(T, P_{H_2}, C_j) \tag{22}$$

$$P_i = (M_{i,tot} - M_i)\frac{RT}{V} \tag{23}$$

$$T = T_0 e^{-\lambda \tau t} \tag{24}$$

$$\frac{dr^3}{dt} = \sum_j \left(\frac{3v_j}{4\pi\eta}\right)\frac{dM_j}{dt} \tag{25}$$

with initial conditions $r = r_O$ and $M_i = M_{i,O}$. $M_{i,tot}$ is the total moles of i in the system, M_i is the moles of i in the condensed phase, and V refers to the volume of the entire closed system. V can be chosen such that when $M_{i,tot}$ is entirely in the gas phase the partial pressure of i is some desired quantity, for example, the partial pressure of i in a solar composition gas of specified total pressure. As before, η is the number of condensate spheres in the volume V. C_j represents a composition vector of the condensed phase required for calculating the saturation vapor pressure of i, and ν_j is the molar volume of each of the j evaporating components that are summed to calculate the changing radius.

The role of the nondimensional parameter ε, which is a measure of whether temperature is changing rapidly or slowly, becomes explicit when the above equations are made nondimensional by measuring time in units of τ_{evap} and the other variables relative to their initial values or the bulk properties of the system (i.e., $t' = t/\tau_{evap}$, $r' = r/r_O$, $M_i' = M_i/M_{i,tot}$, $P_i' = P_i V/M_{i,tot}RT_O$, $T' = T/T_O$, $J_i' = J_i/J_{iO}$ where $J_{i0} = \gamma_i P_{i,sat0}/\sqrt{2\pi m_i RT_0}$ is also the reference flux used to specify ε. $P_{i,sat0}$ is the saturation vapor pressure of i over the starting composition of the condensed phase for $T = T_O$ and specified P_{H_2}. The nondimensional equations (after the usual practice of dropping primes with the understanding that hereafter all variables are nondimensional unless otherwise indicated) become

$$\frac{dM_i}{dt} = -r^2 J_i \tag{26}$$

$$J_i = \Delta P_i e^{-\frac{E}{RT_0}\left(\frac{1}{T}-1\right)} \tag{27}$$

$$P_i = (1 - M_i)T \tag{28}$$

$$T = e^{-\varepsilon t} \tag{29}$$

$$\frac{dr^3}{dt} = \sum_j X_{j0}\frac{dM_j}{dt} \tag{30}$$

In Eqn. 27 $\Delta P_i = (1 - P_i/P_{i,sat})$ where for the purposes of this definition both P_i and $P_{i,sat}$ are dimensional ($P_{i,sat}$ calculated using Eqn. 22). E in Eqn. 27 is an effective activation energy specified such that it takes into account the effect of temperature on both $P_{i,sat}$ and γ_i, and the dependence of J_i on $T^{-1/2}$ from Eqn. 21. X_{j0} is the volume fraction of the j^{th} component in the condensed phase at $t = 0$. Eqns. 26–30 along with Eqn. 22 are the requisite six equations for the six unknowns (M_i, r, J_i, ΔP_i, P_i, and T). The problem becomes fully specified given initial conditions for M_i, $M_{i,tot}$, X_{i0}, r, P_i, and T, two material properties (E and X_{i0}), a thermodynamic model for calculating the saturation vapor pressures (represented here by Eqn. 22), and the dimensionless parameter ε that provides the measure of how fast temperature changes relative to the evaporation or condensation timescales. The main difference in terms of initial conditions between an evaporation calculation and a condensation calculation is that in the former $M_i \approx 1$ and $r \approx 1$ while in the latter $M_i \approx 0$ and $r < 1$ ($r \ll 1$ for $X_{j0} \approx 1$).

4.1. Condensation of Homogeneous Forsterite

In this section the equations derived above are used to model the isotopic fractionation of condensing forsterite as a function of the timescale parameter $\varepsilon = \tau_{cond}/\tau_T$. Forsterite evaporates congruently (see Wang et al., 1999 and references therein), and for present purposes it is assumed that the initial composition of the gas phase is such that only forsterite condenses. Further simplifying assumptions, that will be relaxed in later sections, are that the isotopic composition of the condensed fosterite remains spatially uniform due to rapid transport processes within the condensed phase and that the system composed of the gas plus the condensed phase is closed. It is useful to begin by considering the equilibrium condensation of forsterite in a closed system as this will represent the limiting behavior for sufficiently small ε. The curves without symbols in Figure 7a compare the temperature dependence of the partial pressure of Mg in a solar composition gas ($P = 10^{-3}$ bars at $T = 1773$ K) in the absence of condensation with the saturation pressure of magnesium in equilibrium with forsterite. The continuous curve in Figure 7b is a plot of the fraction of forsterite condensed as a function of the temperature assuming equilibrium. Also shown in these figures are calculated values of P_{Mg} vs. T and the fraction of magnesium condensed (M_{Mg}) vs. T for various choices of ε. As expected, when ε is sufficiently small (e.g., the timescale on which temperature changes is much longer than the condensation timescale) $P_{Mg} \rightarrow P_{Mg,sat}$ and M_{Mg} as a function of temperature approaches that calculated for equilibrium condensation. Figure 7c shows the bulk magnesium isotopic composition of the condensed material for the same choices of ε. When the cooling rate is sufficiently fast compared to the rate of condensation ($\varepsilon > 0.01$) very substantial isotopic fractionation can be produced by partial condensation.

The effect of ε on the isotopic composition of the condensed magnesium is most easily understood in terms of how closely P_{Mg} tracks $P_{Mg,sat}$ for different choices of ε. The effect of $P_{Mg,sat}/P_{Mg}$ on the isotopic fractionation associated with condensation is most easily calculated starting from Eqn. 1 if one assumes that the isotopic composition at the surface is that of the most recently condensed material. The derivation is similar to that for Eqn. 22 in Richter at al. (2002b) with $P_{Mg,sat}/P_{Mg}$ in place of $P_1/P_{1,sat}$ and neglecting any fractionation arising from differences in the diffusivity Mg isotopes in the gas. The result

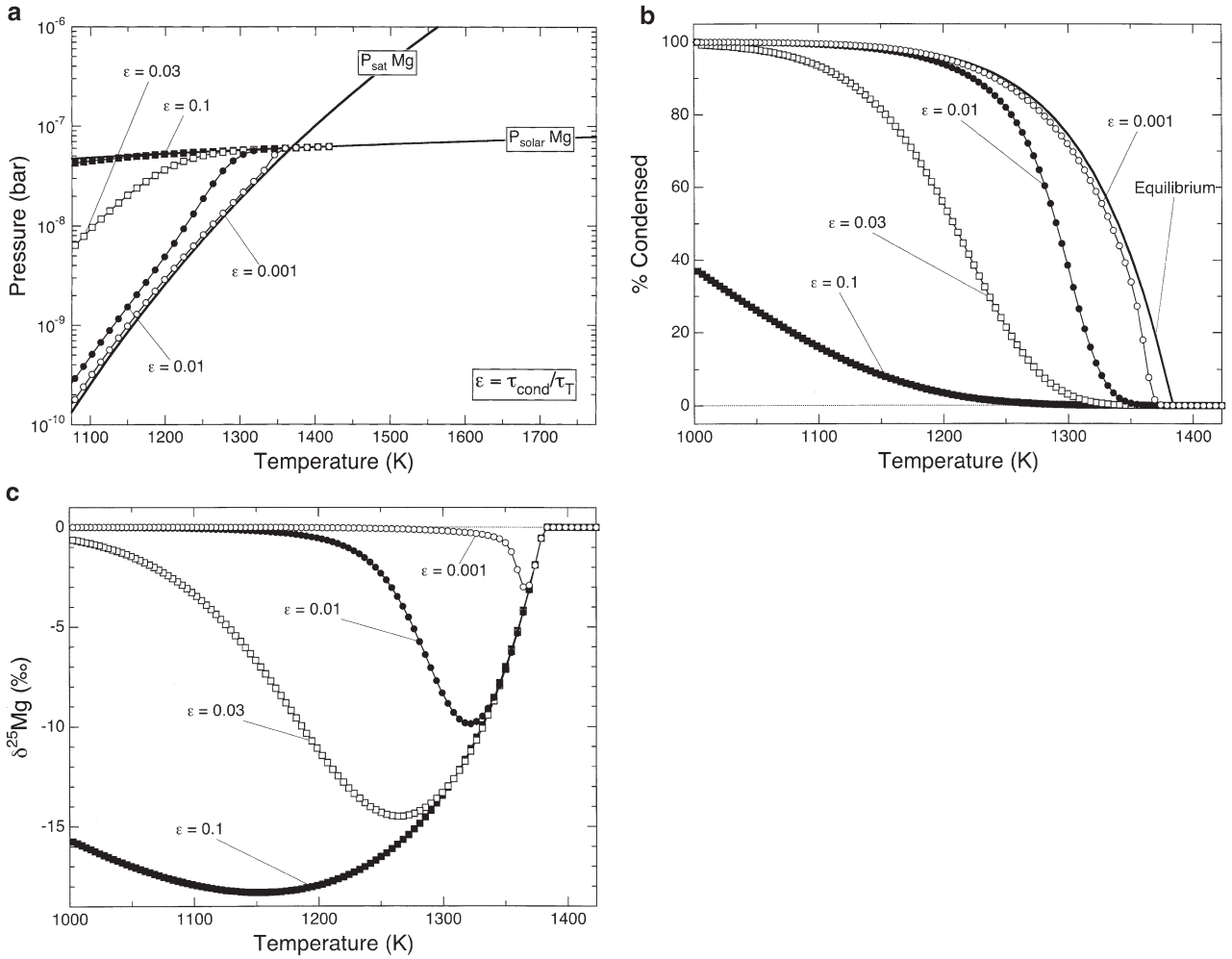

Fig. 7. (a) The thinner continuous curve shows the partial pressure of magnesium as a function of temperature in a solar composition gas of total pressure of 10^{-3} bars if no condensation of magnesium were to take place. The heavier continuous curve is the saturation pressure of magnesium over forsterite as a function of temperature in 10^{-3} bars of hydrogen. The curves with symbols show the calculated partial pressure of magnesium as a function of declining temperature when the rate of temperature change is slow ($\varepsilon \ll 1$) or fast ($\varepsilon \geq 0.1$) compared to the condensation timescale τ_{cond}. $\varepsilon = \tau_{cond}/\tau_T$ where τ_T is the timescale for temperature change defined as the inverse of the e-folding time of the temperature. (b) Fraction of magnesium condensed as forsterite as a function of temperature and the timescale ratio ε. For sufficiently slowly changing temperature ($\varepsilon \leq 0.001$) the fraction of magnesium condensed as a function of temperature approaches that for equilibrium condensation shown by the continuous curve. (c) Magnesium isotopic composition of the condensed phase in per mil relative to the initial $^{25}Mg/^{24}Mg$ in the gas.

phrased in terms of an effective fractionation factor α' for the $^{25}Mg/^{24}Mg$ of the net condensing magnesium is then

$$\alpha' = 1 + (\alpha - 1)\left(1 - \frac{P_{Mg,\,sat24}}{P_{Mg24}}\right) \approx 1 + (\alpha - 1)\left(1 - \frac{P_{Mg,sat}}{P_{Mg}}\right) \tag{31}$$

where $\alpha = \sqrt{24/25}$, $P_{^{24}Mg,sat}$ is the saturation pressure of ^{24}Mg over the condensate, and $P_{^{24}Mg}$ is the partial pressure of ^{24}Mg in the gas. Eqn. 31 shows that the isotopic fractionation of the earliest condensing magnesium will always be small when condensation begins with $P_{Mg} \approx P_{Mg,sat}$. This explains why the highest temperature condensates in Figure 7c are unfractionated regardless of ε. If however the temperature falls sufficiently quickly ($\varepsilon \to 1$) the ratio $P_{Mg,sat}/P_{Mg}$ soon becomes negligible compared to 1 (see Fig. 7a) and the condensate can become isotopically fractionated to the fullest extent possible (i.e., $\alpha' = \alpha$). The isotopic fractionation must vanish once all the magnesium has condensed, which explains why the fractionations shown in Figure 7c evolve back towards zero as the percent of magnesium condensed (shown in Fig. 7b) tends to 100%.

4.2. Evaporation of a Homogeneous CAI-like Liquid

This section describes model problems motivated by the Type B CAIs. The results illustrate the effect of the rate of change of the temperature on the elemental and isotopic fractionation of magnesium evaporating from a Type B CAI-like liquid when diffusion in the liquid and surrounding gas is

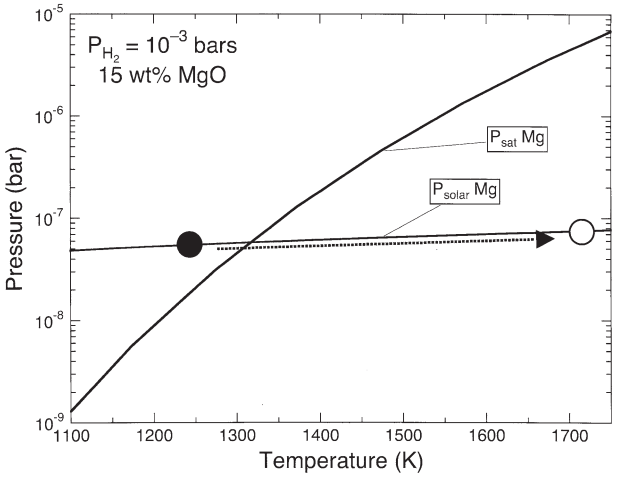

Fig. 8. The two curves plotted as unbroken lines show the partial pressure of magnesium in a solar composition gas of total pressure 10^{-3} bars (assuming no condensation) and the saturation vapor pressure of magnesium over a Type B CAI-like liquid in 10^{-3} bars of hydrogen as a function of temperature. The dashed curve shows a trajectory for rapid reheating of an initially solid Type B CAI-like composition (black circle) to a temperature where it becomes ~95% partially molten (open circle). The open circle is the initial conditions for T and P_{Mg} used in the evaporation calculations of a Type B CAI-like liquid discussed in the text.

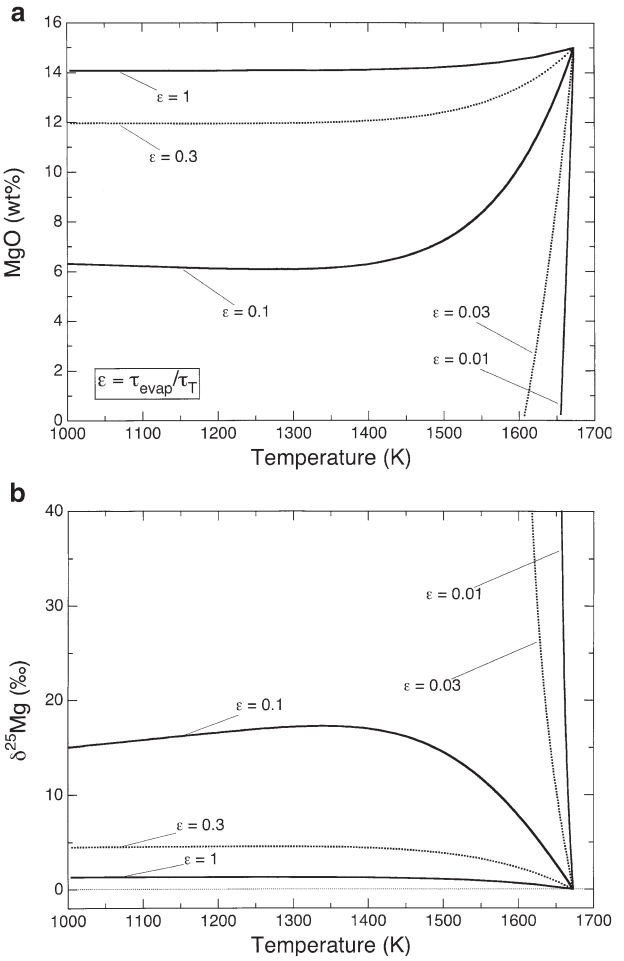

Fig. 9. (a) MgO content of evaporation residues plotted as a function of temperature for calculations starting with 15 wt% MgO and cooling from 1673 K at different rates specified by $\varepsilon = \tau_{cond}/\tau_T$, where τ_{cond} is the condensation timescale and τ_T is the timescale for temperature change as defined in the text. (b) Magnesium isotope fractionation in per mil corresponding to the five cases shown in (a).

sufficiently fast that both can be considered to be homogeneous at all times. The gas plus condensed phase are assumed to be a closed system. The initial composition considered in this section is that of the partial condensate of a solar composition gas to the point ($T \approx 1300$ K and $P \approx 10^{-3}$ atm) where ~5% of the total magnesium has condensed. The condensate will have ~15% wt % MgO. This partial condensate is then rapidly reheated by some unspecified process (perhaps a shock wave as discussed by Desch and Connolly, 2002) to a temperature of ~1700 K sufficient to produce 95% partial melting with only a few spinel crystals remaining. As mentioned earlier, such a large degree of partial melting is indicated by the coarse-grained texture of the Type B CAIs. Figure 8 illustrates the effect of rapid reheating in terms of producing significant undersaturation of the magnesium component in the gas at 1700 K. Unless the subsequent cooling is extremely fast compared to the timescale for evaporation, this undersaturation will result in the preferential evaporation of some of the magnesium relative to the much more refractory calcium and aluminum. The model calculations for the evaporation of magnesium from a reheated Type B CAI-like composition involve numerical integration of Eqns. 26–30 along with a thermodynamic model for the solution properties of the melt. The thermodynamic model used here to calculate the saturation vapor pressures was developed by Denton Ebel for the evaporation calculations discussed in Grossman et al. (2000) and in Richter et al. (2002b).

Figure 9 shows model results for the effect of the cooling rate, specified in terms of the temperature change parameter $\varepsilon = \tau_{evap}/\tau_T$ on the elemental and isotopic fractionation of magnesium from a model Type B CAI. When the cooling rate is sufficiently slow (i.e., $\varepsilon \leq 0.03$) all the magnesium not in crystallized phases (mostly spinel) will have evaporated by the time the temperature has dropped by a few tens of degrees. The isotopic fractionation during evaporation in this limit follows a Rayleigh curve as given by Eqn. 11. In the opposite limit ($\varepsilon > 1$), the cooling rate is so fast that both elemental and isotopic fractionations are negligible for lack of time.

The model calculations discussed in sections 4.1 and 4.2 show that isotopic fractionation can take place during either partial evaporation or during partial condensation depending on the value of ε, which measures how much temperature changes on the timescale over which significant evaporation or condensation can take place. In the case of condensation during cooling, when $\varepsilon < 1$ (i.e., temperature changing slowly compared to the time it takes to condense the species of interest) systems will remain close to equilibrium and there will be very little isotopic fractionation. As $\varepsilon \rightarrow 1$, systems increasingly depart from equilibrium by becoming supersaturated and producing condensates enriched in the lighter isotopes of the evaporating species. In the case of evaporation of a molten condensate following rapid reheating, the system starts out undersaturated and for $\varepsilon < 1$ the residue becomes enriched in

the heavy isotopes of the evaporating species. When the cooling rate is sufficiently fast compared to evaporation (i.e., $\varepsilon > 1$) both the elemental and the isotopic fractionations are negligible.

5. DIFFUSION-LIMITED EVAPORATION AND CONDENSATION

In the preceding section it was assumed that the condensed phase remained homogeneous despite elemental and isotopic fractionation at the surface, implying that chemical transport processes were fast compared to the evaporation or condensation timescale. Here we will relax the requirement that the phases remain homogeneous at all times. The timescale for chemical homogenization of the condensed phase by diffusion, τ_D, will be of the order of $\tau_D = L^2/D$, where L is a typical length scale (e.g., radius for a sphere or half thickness for a slab) and D is the chemical diffusion coefficient. The condensed phase will be effectively homogenized if this timescale is short compared to the evaporation or condensation timescale. The nondimensional parameter that will determine the degree of homogeneity of component i in the condensed phase will be of the form $\tau_D/\tau_{evap} = (L^2/D)/(M_i/J_iA) = nLJ_i/C_iD$ where A is the surface area, M_i is the total moles of i in the condensed phase, C_i is the molar density of i, and n is now used to represent a geometrical factor that specifies the surface to volume ratio of the geometry considered ($n = 3$ for a sphere with radius $r = L$, $n = 1$ for a slab of half thickness L). We can already anticipate that when τ_D/τ_{evap} is large, diffusion will be too slow for the condensed phase to remain homogeneous during evaporation or condensation.

To model departures from homogeneity due to finite chemical diffusion rates in the condensed phase Eqn. 26 needs to be replaced by a partial differential equation and appropriate boundary conditions. For the sake of simplicity, and because certain analytical solutions are then more easily obtained, the case consider here will involve a horizontally uniform slab. The dimensional mass conservation equations become

$$\frac{\partial C_i}{\partial t} + U\frac{\partial C_i}{\partial x} = D_i\frac{\partial^2 C_i}{\partial x^2} \tag{32}$$

where x is the distance coordinate normal to the surface, U is an advection velocity that depends on the frame of reference (e.g., $U = 0$ for a frame attached to the center of the slab, $U \neq 0$ for a frame attached to one of the evaporating or condensing surfaces of the slab) and D_i is an effective binary diffusion coefficient for the component containing i. In the reference frame attached to the center of the slab at $x = 0$, the boundary conditions in terms of dimensional variables become

$$\frac{\partial C_i}{\partial x} = 0 \quad \text{at} \quad x = 0 \tag{33}$$

$$D_i\frac{\partial C_i}{\partial x} + UC_i = -J_i \quad \text{at} \quad x = \pm L(t) \tag{34}$$

U in boundary condition 34 is the velocity of the surface at $L(t)$ relative to the center of the slab, which in the reference frame used will be a negative velocity. For a sufficiently thick slab (thick compared to the distance affected by diffusion over the time of interest) the reference frame can be attached to either of the moving surfaces of the slab. In this frame of reference the surface of interest can be called $x = 0$ and material from the interior ($x \rightarrow \infty$) will be continuously advected towards the surface with velocity U. Boundary conditions 33 and 34 are still used in the moving reference frame but with Eqn. 33 applied at $x \rightarrow \infty$ and Eqn. 34 at $x = 0$. The velocity U of the surface relative to the center of the slab depends on the evaporation or condensation fluxes J_k as

$$U = \sum\nolimits_k \nu_k J_k \tag{35}$$

where ν_k is the molar volume of component k. For present purposes it is most natural to nondimensionalize time in terms of the diffusion timescale, thus $t' = t/\left(L_0^2/D_0\right)$, and also $x' = x/L_0$, $L' = L/L_0$, $C'_i = C_i/C_{i0}$, $J'_i = J_i/J_{i0}$, $U' = U/U_0$, and $D'_i = D_i/D_0$. L_0 is a typical dimension (e.g., the initial half thickness of a slab), D_0 is a measure of the magnitude of the diffusion coefficients, C_{i0} is some appropriate measure of the molar density of component i in the condensed phase (e.g., the initial value in the condensed phase), and U_0 is the velocity of the boundary when the fluxes J_k are equal to their reference value J_{k0}. The nondimensional equivalents of Eqns. 32 and 35 and the boundary conditions 33 and 34 are (after dropping the primes)

$$\frac{\partial C_i}{\partial t} + PeU\frac{\partial C_i}{\partial x} = D_i\frac{\partial^2 C_i}{\partial x^2} \tag{36}$$

$$U = \frac{\sum_k \nu_k J_{k0} J_k}{\sum_k \nu_k J_{k0}} \tag{37}$$

$$\frac{\partial C_i}{\partial x} = 0 \quad \text{at} \quad x = 0 \tag{38}$$

$$D_i\frac{\partial C_i}{\partial x} = PeUC_i - E_iJ_i \quad \text{at} \quad x = \pm L(t) \tag{39}$$

where Pe ($=U_0L_0/D_0$) is the Peclet number and E_i ($=J_{i0}L_0/D_0C_{i0}$), which Richter et al. (2002b) called the evaporation number for component i, is the ratio of the diffusion timescale τ_D to the evaporation timescale τ_{evap} of component i. Using the definition of U_0 in the Peclet number, one derives the following relationship between the Peclet number and the evaporation numbers.

$$Pe = \frac{L_0}{D_0}\sum\nolimits_k \nu_k J_{k0} = \sum\nolimits_k C_{k0}\nu_k\left(\frac{J_{k0}L_0}{D_0C_{k0}}\right) = \sum\nolimits_k V_kE_k \tag{40}$$

where V_k is the initial volume fraction of the kth component. Using Eqn. 39, the all-important boundary condition 40 can be rewritten in terms of the evaporation numbers as

$$D_i\frac{\partial C_i}{\partial x} = UC_i\sum\nolimits_k V_kE_k - E_iJ_i \quad \text{at} \quad x = \pm L(t) \tag{41}$$

Note that congruent evaporation (i.e., $k = 1$) is a special case in that the right hand side of Eqn. 41 becomes equal to zero to reflect the fact that no chemical gradients can arise in a congruently evaporating system. For the more general case of multicomponent systems, the right hand side of boundary con-

dition 41 as it applies to a given component can be either positive or negative depending on the relative volatility and abundance of the various components. The model problems discussed in the following sections involving diffusion-limited condensation or evaporation are based on Eqns. 36 and 37 subject to boundary conditions 38 and 41, together with Eqns. 27–29, and constitutive equations for calculating the reference evaporation or condensation fluxes J_{k0} and the diffusion coefficients D_i.

5.1. Diffusion-Limited Condensation of Forsterite

The major magnesium-containing phase to condense from a solar composition gas at the pressures usually assumed for the early solar nebula is solid forsterite (Grossman, 1972; Yoneda and Grossman, 1995). Forsterite evaporates congruently and for the purpose of this section the initial composition of the gas is assumed to be such that condensation can also be characterized in terms of forsterite alone. In the limit of a one-component system, boundary condition 41 becomes simply $\partial C_i/\partial x = 0$, and $C_i = 1$ is then a solution valid for all times. The isotopic composition of the condensate can still be fractionated if condensation takes place from a supersaturated gas. The model problem for condensation of homogeneous forsterite discussed in Section 4.1 can now be seen to involve the limit $E_i \rightarrow 0$. However, diffusion in solid forsterite is sufficiently slow that condensation from a supersaturated state onto a finite size object ($L > 1$ μm) will almost certainly be in the opposite limit, $E_i \gg 1$. For example, $E_{Mg} \approx 100$ for $L = 1$ μm ($E_{Mg} \approx 10^5$ for $L = 1$ mm) using the forsterite evaporation timescales for $P_{H_2} = 10^{-3}$ atm and $T \approx 1400$ K given in Figure 6 and the magnesium diffusivities as a function of temperature given in Figure 4 of Wang et al. (1999). When $E_i \gg 1$, using L_0^2/D_0 to scale time is no longer particularly useful, instead time is better measured in units of the condensation time $C_{i0}L_0/J_{i0}$. When this is done, the diffusion term on the right hand side of Eqn. 36 becomes of order E_i^{-1}, indicating that for sufficiently large E_i transport by diffusion can be neglected.

The main difference between the isotopic fractionation of the condensed phase in the limit $E_i \ll 1$ vs. $E_i \gg 1$ is that in the former case the isotopic composition will be spatially uniform whereas in the latter, the isotopic composition will be zoned reflecting that each increment of condensation does not exchange with earlier condensed increments. However, the bulk isotopic composition of the condensate is not much affected by E_i, as can be seen in Figure 10 showing calculated magnesium isotopic compositions of forsterite condensing onto a sphere as a function of radius and a rate of temperature change given by $\varepsilon = \tau_{cond}/\tau_T = 0.1$ (i.e., temperature changing sufficiently fast to allow for significant isotopic fractionation). A spherical geometry is used here because the profiles vary more smoothly with radius than they would with the thickness of an equivalent slab. The figure shows that the bulk isotopic composition of the condensed forsterite for $E_i \gg 1$ is not much different from that of a homogeneous sphere ($E_i \ll 1$) evaporating with the same value of ε. The overall conclusion is that the parameter $E_i = \tau_D/\tau_{cond}$ has little effect on the bulk isotopic composition of the condensed phase, but for E_i large (i.e., slow diffusion), the condensed phase will be zoned reflecting the isotopic composition of each increment of condensate.

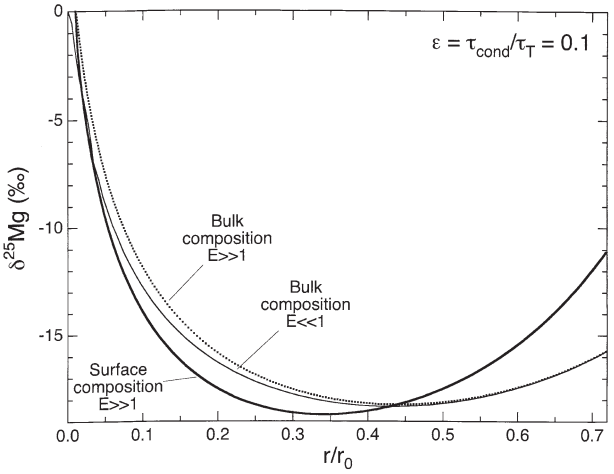

Fig. 10. Calculated magnesium isotopic composition of condensates from a system cooling at $\varepsilon = 0.1$ in the homogeneous condensate limit ($E \ll 1$) and in the completely diffusion-limited case ($E \gg 1$) plotted as a function of the fractional radius of a sphere that would have a final radius r_0 once all the magnesium has condensed. The bulk composition of the diffusion-limited sample (dotted curve labeled $E \gg 1$) is not significantly different from that of the homogeneous sample shown by the thin continuous curve labeled $E \ll 1$.

5.2. Diffusion-Limited Evaporation of Forsterite

Forsterite evaporates congruently and so the only reason to model diffusion-limited conditions is to investigate the effect in terms of isotopic fractionation. Wang (1995; see also Wang et al., 1999) has already discussed this problem in some detail in the limit $P_i/P_{i,sat} \ll 1$ (i.e., free evaporation) and provided both a time-dependent analytical solution for the isotopic ratio and experimental data in excellent agreement with the eventual steady state solution that develops in the frame of reference attached to the evaporating surface. Here I will also assume that $P_i/P_{i,sat} \ll 1$ but seek a slightly more general solution to this problem in terms of the individual isotopes. Assuming that a steady state exists, (i.e., $\partial T_i/\partial t = 0$, $\partial C_i/\partial t = 0$ and D_i, U, and J_i all equal to 1), Eqn. 36 becomes

$$Pe\,\frac{\partial C_i}{\partial x} = \frac{\partial^2 C_i}{\partial x^2} \tag{42}$$

subject to the boundary condition

$$\frac{\partial C_i}{\partial x} = PeC_i - E_i \quad \text{at} \quad x = 0 \tag{43}$$

where C_i and its initial value C_{i0} are now being used to represent the fraction of isotope i relative to the sum of all isotopes of the element of interest. The initial isotope ratio is then defined as $R_0 = C_{20}/C_{10}$. J_0 is used to represent the total free evaporation flux of the element of interest if it were composed entirely of isotope *1*. The flux of the individual isotopes *1* and *2* is then $J_1 = C_1J_0$ and $J_2 = \alpha C_2J_0$ using the value of C_i at the evaporating surface and $\alpha = \sqrt{m_1/m_2}$. This results in $E_1 = C_1J_0L_0/C_0D_0$, $E_2 = \alpha RE_1$, and $Pe = E_1 + E_2$.

The steady state solution of Eqn. 42 is of the form

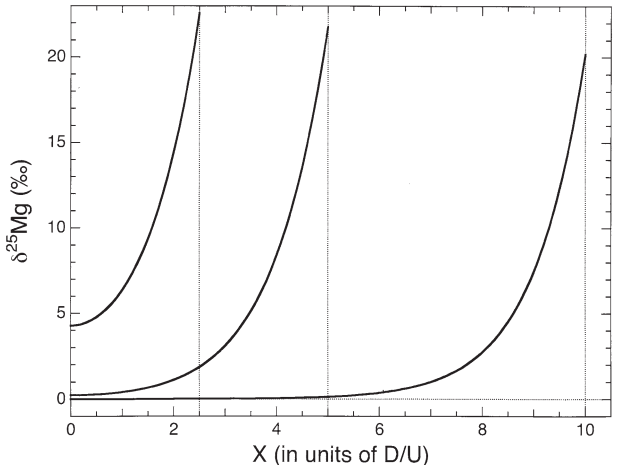

Fig. 11. Profiles of the magnesium isotopic composition from a model calculation of an evaporating slab of forsterite in the diffusion-limited regime. Three cases are shown corresponding to slab half thicknesses that have evolved to $x = 10$, 5, and 2.5 in units of D/U where D is the diffusion coefficient for magnesium isotope exchange in forsterite and U is the velocity of the surface relative to the center due to evaporation. For $x \geq 10$, the magnesium isotopic profile is unchanging in a reference frame attached to the moving surface.

$$C_i = C_{i0} + \chi_i e^{-Pex} \tag{44}$$

which in order to satisfy the boundary condition (Eqn. 43) requires

$$\chi_1 = \frac{(\alpha - 1)C_{10}C_{20}}{\alpha C_{10} + C_{20}} \tag{45}$$

$$\chi_2 = \frac{(1 - \alpha)C_{10}C_{20}}{\alpha C_{10} + C_{20}} \tag{46}$$

Thus the faster (slower) evaporating isotope decreases (increases) towards the surface by an amount of order $(\alpha - 1)$ over a nondimensional distance of order Pe^{-1} corresponding to a dimensional distance D_O/U. At steady state, the isotopic ratio at the evaporating surface is $R = R_O/\alpha$. The time for this steady state to become established is of the order of the time required to diffuse over a distance D_O/U, which is D_O/U^2 or equivalently τ_{evap}/Pe. Figure 11 shows the steady state solution for the isotopic ratio in terms of the departure of the $^{25}Mg/^{24}Mg$ ratio (expressed as δ^{25}Mg in ‰) from the initial value. This solution will be unchanging in a frame attached to the evaporating surface until the dimensions of the slab become less than $\sim 10\, D_O/U$. Also shown are two magnesium isotopic profiles for times when the slab is no longer effectively large compared to the boundary layer. A reasonable estimate of the bulk isotopic fractionation of a layer that has been reduced by evaporation to a fractional half thickness L is $\delta^{25}\text{Mg} \approx 1000(1 - \alpha)\, \text{L}^{-1}\, \text{Pe}^{-1}$, valid for $Pe > 10$ and $LPe > 5$.

5.3. Diffusion-Limited Evaporation of a CAI-like Liquid

Richter et al. (2002b) have already discussed the isotopic fractionation magnesium due to free evaporation from a CMAS liquid sphere for initial evaporation numbers in the range $E_{Mg} = 0$ (ideal Rayleigh fractionation) to $E_{Mg} = 10$ (see their fig. 14). For $E_{Mg} > 1$, significant chemical and isotopic gradients develop and there is a systematic decrease in the bulk isotopic fractionation for a given amount of magnesium evaporated. For example, figure 14d in Richter et al. (2002b) shows that δ^{25}Mg when 50% magnesium has evaporated decreases as a function of E_{Mg} as $e^{-0.09E_{Mg}}$. Here the effect of even smaller evaporation numbers during free evaporation will be considered using a model that is simplified in several ways from that given in Richter et al. (2002b). The model assumes the condensed phase to be a slab rather than a sphere as this will allow the results to be more easily confirmed by analytical solutions. The system will be treated as effectively binary by considering MgO + Σ(CaO + Al_2O_3 + SiO_2) with only the MgO component evaporating. Chemical diffusion is then characterized by a single effective binary diffusion coefficient for MgO. The model assumes that the activity of the MgO component in the melt is proportional to the mole fraction of MgO in the melt and that the system remains completely molten at all times. These simplifications, which do not compromise the qualitative behavior of the system, are made in order that one might more easily understand a particularly surprising aspect of the isotopic fractionations produced by this model. The results of the present simplified model have been compared in several cases to those of the more complete four-component spherical model with realistic thermodynamic solution properties of Richter et al. (2002b) and the differences in terms of the calculated bulk properties are indeed quite minor.

Figure 12 shows various aspects of the results of an evaporation calculation with an initially large evaporation number $E_{Mg} = 100$. Figure 12a shows the magnesium concentration as a function time measured in units of L^2/D where L is the half thickness of the layer and D is the effective binary diffusion coefficient of the MgO component in the melt. Diffusion-limited evaporation of a relatively minor component such as MgO (initially 10 wt% in this calculation) rapidly reduces the concentration of that component at the evaporating surface to the point that the rate of evaporation, which is proportional to the MgO concentration at the surface, becomes sufficiently small that diffusion can continuously replenish the loss of magnesium from the surface. In other words, regardless of the initial conditions, the evaporation number rapidly becomes of order one. A remarkable feature of model results for E_{Mg} initially equal to 100 is shown in Figure 12b. The isotopic fractionation of magnesium remains restricted to a thin boundary layer at the surface even when the elemental fractionation has affected the interior of the slab to the point of having removed almost all of the initial magnesium. Ozawa and Nagahara (2001) have also found a similar result in their very detailed model calculations of evaporation effects in a molten binary system. The very different spatial distribution of the elemental and isotopic fractionations as well as its cause is sufficiently puzzling that an even simpler model problem was posed in an effort to gain some additional insight. The simplified model involves a half-space with the velocity of the surface set to zero despite evaporation from the surface. This represents a legitimate limiting situation in that the surface velocity will become negligible if the evaporating components are sufficiently dilute so that they represent a negligible volume fraction of the system as a whole (i.e., $Pe \rightarrow 0$ as $V_k \rightarrow 0$). The evaporation problem in the limit $Pe \rightarrow 0$, $E_{Mg} \neq 0$ is equivalent to that of temperature in a slab cooled by a radiation boundary

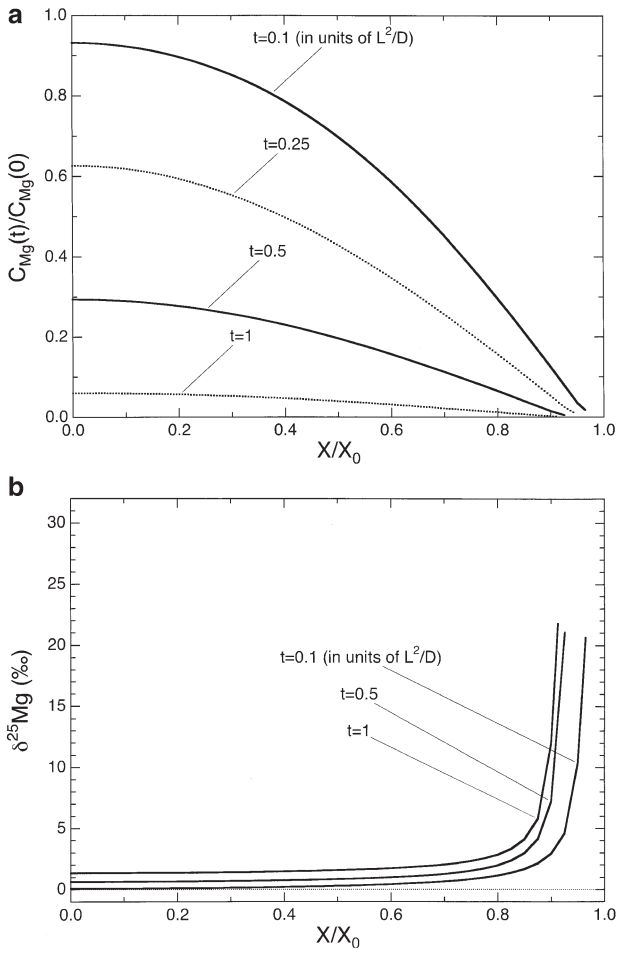

Fig. 12. (a) Profiles of the MgO content (measured as a fraction of the initial amount) of an evaporating CMAS liquid slab at four different times. Time is measured in units of τ_D, the diffusion time scale. The magnesium evaporation number, E_{Mg}, is initially equal to 100, but soon falls to about one as the evaporation rate decreases in proportion to the reduced MgO content at the evaporating surface. (b) Magnesium isotopic composition profiles for three of the times used in panel (a). A noteworthy feature of the results is that the isotopic fractionation remains restricted to a surface boundary layer even when the MgO content of the interior has been reduced to less than 10% of the initial amount.

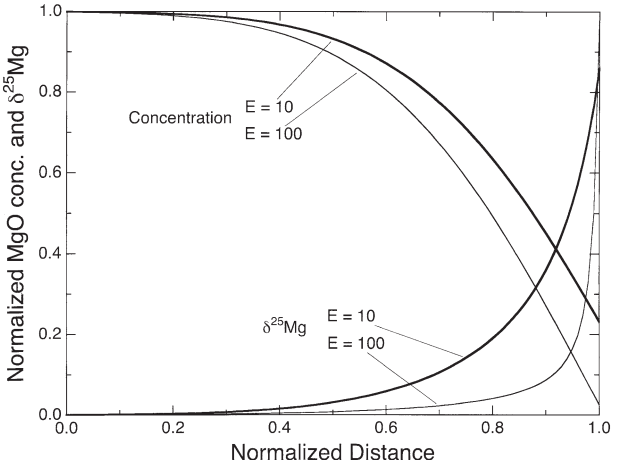

Fig. 13. Normalized MgO concentration and isotopic composition profiles from an analytical solution for magnesium evaporation from a CMAS liquid slab with initial evaporation numbers of 10 and 100. The model used for this case differs from that used to construct Figure 12 in assuming that the surface velocity can be neglected and set to zero.

condition with the surface flux proportional to the surface temperature. The solution for this radiation problem is given in Carslaw and Jaeger (1959) and in terms of the variables used here it becomes

$$\frac{C(t)}{C(0)} = erf\left(\frac{x}{2\sqrt{t}}\right) + e^{E_{Mg}x+E_{Mg}^2 t}erfc\left(\frac{x}{2\sqrt{t}} + E\sqrt{t}\right) \quad (47)$$

E_{Mg} represents either $E_{^{24}Mg}$ or $E_{^{25}Mg}$ depending on whether C in Eqn. 47 refers to the concentration of ^{24}Mg or ^{25}Mg. Figure 13 shows the result of using Eqn. 47 to calculate the evolution of ^{24}Mg and ^{25}Mg due to evaporation from the surface with $E_{^{24}Mg}$ = 10 and 100, and $E_{^{25}Mg} = \sqrt{24/25}\, E_{^{24}Mg}$. In much the same way as was seen earlier in Figure 12, Figure 13 shows the isotopic fractionation restricted to a boundary layer while the elemental profiles are diffused over a significantly larger distance. This result is a reminder that the equation governing the time evolution of an isotopic ratio is not a diffusion equation, although it is very often approximated as such. Consider the equation for two isotopes with molar density C_1 and C_2, each obeying a diffusive mass conservation equation of the form

$$\frac{\partial C_i}{\partial t} = \frac{\partial^2 C_i}{\partial x^2} \quad (48)$$

The equation for the ratio $R = (C_2/C_1)$ is obtained by first expanding the time derivative $\partial(C_2/C_1)/\partial t$ and then using Eqn. 48 to write the result in terms of R and C_1. The result is

$$\frac{\partial R}{\partial t} = \frac{\partial^2 R}{\partial x^2} + \frac{2}{C_i}\frac{\partial C_i}{\partial x}\frac{\partial R}{\partial x} \quad (49)$$

The second term on the r.h.s. of Eqn. 48 plays the role of an advection term (i.e., a term like $u(\partial R/\partial x)$ with effective velocity $u = -(2/C_1)(\partial C_1/\partial x)$) that for $(\partial C_1/\partial x)$ positive will maintain a boundary layer by offsetting the effect of the diffusion term in much the same way that an actual velocity gave rise to a steady state boundary layer solution in the congruent evaporation case. As can be seen in Figure 13, the smaller C_1 becomes at the surface, the narrower the boundary layer becomes because the "advection velocity" is proportional to $1/C_1$.

One might, at this point, be tempted to conclude that diffusion-limited evaporation of volatile species from a multi-component condensed phase can significantly fractionate elements by volatility without very much bulk isotopic fractionation of the residue. To conclude this would, however, ignore the possibility of isotope fractionation by chemical diffusion in silicate melts. Richter et al. (1999, 2003) showed that chemical diffusion in silicate melts fractionates calcium isotopes by an amount that corresponds to a mass dependence of the diffusion coefficients of the individual isotopes of $D_1/D_2 = (m_2/m_1)^\beta$ with $\beta \approx 0.1$. Richter et al. (2003) also showed that lithium isotopes were fractionated during chemical diffusion in a way corresponding to $\beta \approx 0.2$. Tsuchiyama et al. (1994) used

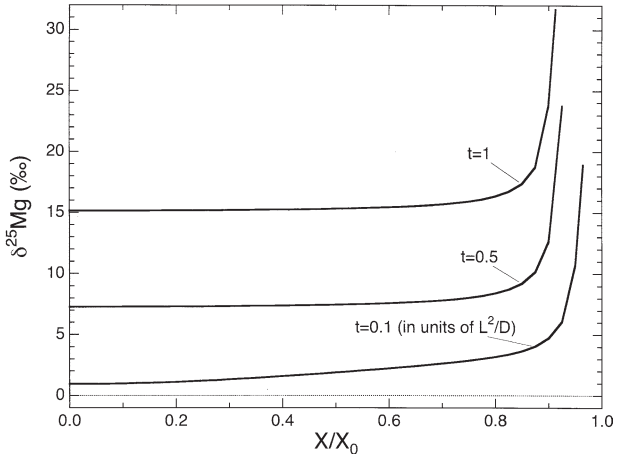

Fig. 14. Same as Figure 12b except that in calculating the magnesium isotopic profiles shown here it was assumed that the magnesium isotopes have slightly different diffusion coefficients given by $D_{25_{Mg}}/D_{24_{Mg}} = (24/25)^{0.1}$.

molecular dynamic simulations to calculate a value of $\beta = 0.1$ for magnesium isotopes diffusing in molten MgO. These experimental and computational results make it very likely that the diffusion of magnesium in a CMAS liquid will fractionate magnesium isotopes by an amount corresponding to $\beta \approx 0.1$. Figure 14 shows model results for the isotopic fractionation of magnesium in evaporation residues when diffusive isotope fractionation with $\beta \approx 0.1$ is included in the calculation used earlier to construct Figure 12. The magnesium concentration profiles from this new calculation are unchanged from those shown in Figure 12a, however the isotopic composition of the interior is now very significantly fractionated by $t = 0.5$. This is because in the diffusion-limited evaporation regime the magnesium being lost from the surface has to be replenished by diffusion from the interior, and as a result of the lighter isotope diffusing faster, the interior isotopic composition becomes progressively heavier. So, it seems very likely that diffusion-limited evaporation of a multicomponent system will produce isotopically fractionated residues after all.

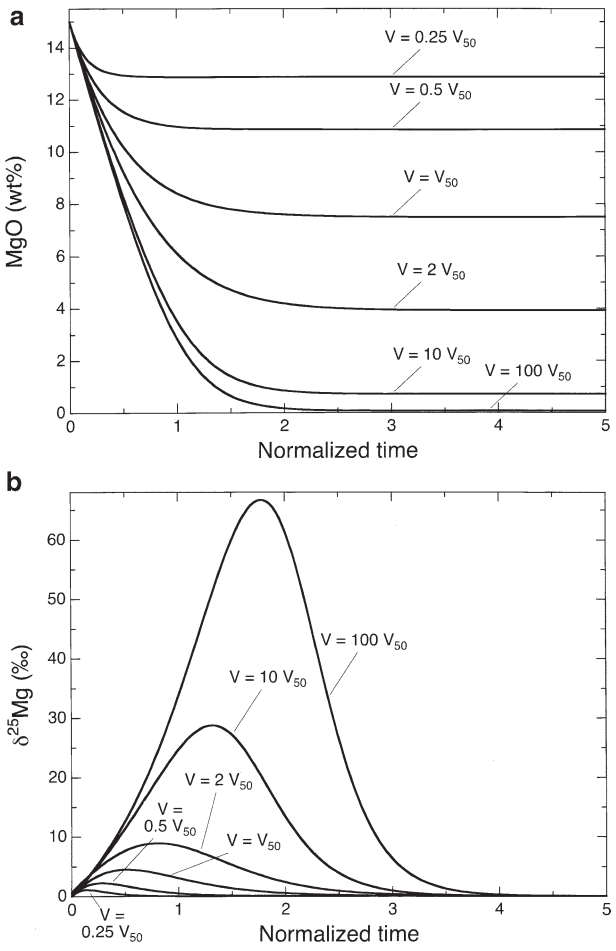

Fig. 15. (a) Wt% MgO as a function of time in a CMAS condensed phase evaporating into a fixed closed volume V measured in units V_{50} defined as the volume such that when the gas and condensed phase are in equilibrium, 50% of the of the magnesium will be in each phase. Time is measured in units of the evaporation timescale τ_{evap}. (b) Evolution of the magnesium isotopic composition of the condensed phase as a function of time for the six cases shown in (a).

6. OPEN AND CLOSED SYSTEMS

The model calculations in this section address the effects in terms of elemental and isotopic fractionation of evaporating systems being partially open to gas loss. The limiting case of a perfectly closed system will serve as a starting point with which to consider the effect of removing the evaporating species from the surrounding gas at a finite rate, and eventually sufficiently rapidly that the behavior approaches that of the perfectly open system. The model problems involve the evaporation and recondensation of the magnesium content of a molten sphere at a fixed temperature T = 1673 K with a stating composition 15 wt% MgO, 36 wt% SiO_2, 27 wt% CaO, and 22 wt% Al_2O_3. The initial conditions assume that all the material starts out in the condensed phase. A key parameter in the model is the ratio of the total mass of the condensed phase to the total volume of the system, which will determine the wt% MgO remaining in the condensed phase once the system achieves equilibrium. A recent very detailed discussion of the isotopic fractionation in a cooling closed system with realistic solar bulk composition (but without crystallization, which was emphasized in an earlier discussion by Grossman et al., 2002) is given by Grossman and Fedkin (2003).

The first set of model calculations assume that a homogeneous condensed phase and a well-mixed surrounding gas occupy a fixed volume at a constant temperature. The rate of change of the moles of magnesium initially all in the condensed phase of radius r and in a surrounding gas of fixed volume V is calculated using Eqn. 1 for the magnesium flux J_{Mg} with $\gamma_{Mg} = 0.03$ (from Richter et al., 2002b), $P_{Mg,sat}$ from the thermodynamic model described in Grossman et al. (2000), and P_{Mg} calculated using the ideal gas law. Time is measured in units of $\tau_{evap} = M_{Mg}/4\pi r^2 J_{Mg}$ where M_{Mg} is the total moles of magnesium in the system and J_{Mg} is the magnesium flux when all the magnesium is still in the condensed phase. Figure 15 shows the effect of different choices for the total volume of the closed system on the time evolution of the MgO content and magnesium isotopic composition of the condensed phase. In these

calculations the total volume of the system is measured in terms of a reference volume (V_{50}) defined as the volume such that at equilibrium there would be equal amounts of magnesium in the gas and in the condensed phase. As expected, Figure 15a shows that the smaller the volume the less magnesium is lost by the condensed phase to establish equilibrium with the surrounding gas. Figure 15b shows the corresponding magnesium isotopic composition of the condensed phase for the various choices of the volume of the system. The larger the total volume of the system, the greater the maximum isotopic fractionation, however, given sufficient time, the continuous exchange of magnesium with the surrounding gas drives the isotopic fractionation back to zero. An important if somewhat obvious conclusion is that even when only a very small fraction of the volatile species remains in the condensed phase (<1% of the original amount), the isotopic composition of the condensed phase returns to normal on a time scale short compared to ten times τ_{evap}.

Partially open systems will be characterized in terms of a decay constant λ corresponding to the fraction of the species of interest in the gas removed per unit time by some process other than recondensation. A finite flow of the surrounding gas relative to the condensed materials is an example of such a partially open system. A residence timescale in the surrounding gas can be defined in terms of the decay constant as $\tau_R = 1/\lambda$. The model problem for magnesium in a partially open system differs from the closed system model in that the partial pressure of magnesium, P_{Mg}, is reduced every time increment Δt by a fraction $P_{Mg}\lambda\ \Delta\ t$ with $\Delta\ t$ and λ measured in units of τ_{evap}. Figure 16 shows that when the rate of removal of magnesium from the gas is sufficiently fast compared to evaporation (i.e., short residence time with $\tau_{evap}/\tau_R > 10$) the MgO content decreases much as it would for free evaporation into a vacuum and the magnesium isotopic fractionation of the residue tends to the corresponding ideal Rayleigh fractionation limit. When the rate of removal of magnesium from the gas is slow (i.e., $\tau_{evap}/\tau_R < 0$) the MgO content and the isotopic composition of the residue at early times are similar to that in the closed system ($\tau_{evap}/\tau_R = {}_0$), but for longer times, the slow but finite rate of magnesium loss from the system will result in a perceptible decline of the MgO content of the residue and small but finite isotopic fractionation.

The problems so far considered in this section have assumed that the surrounding gas is well mixed in terms of the distribution of the evaporating species. If however, the total pressure of the surrounding gas is sufficiently high that diffusion through this gas has to be taken into account, the removal of evaporating species from the vicinity of the surface will require that there be a greater pressure of the evaporating species at the evaporating surface compared to that in the far field. In the case of the far-field partial pressure of the evaporating species being negligible compared to the saturation vapor pressure, the surface pressure P_i relative to the saturation pressure $P_{i,sat}$ is given by (see Richter et al., 2002b)

$$\frac{P_i}{P_{i,sat}} = 1 - \frac{1}{1 + \dfrac{\gamma_i r}{D_i^{gas}}\sqrt{\dfrac{RT}{2\pi m_i}}} \tag{50}$$

where r is the radius of the condensed phase and D_i^{gas} is the binary diffusion coefficient for the species of interest through the surrounding gas. The effect of the pressure of the surrounding gas enters via its effect on the diffusivity of the evaporating species (i.e., the diffusion coefficient is inversely proportional to the total gas pressure). The finite pressure at the surface produces recondensation, which slows the net evaporation rate and reduces the kinetic isotope fractionation. The reduction of the net evaporation rate relative to the free evaporation rate is given by

$$J_{i,net}/J_i = \frac{1}{1 + \dfrac{\gamma_i r}{D_i^{gas}}\sqrt{\dfrac{RT}{2\pi m_i}}} \tag{51}$$

Richter et al. (2002b) also derived a relationship for the effect

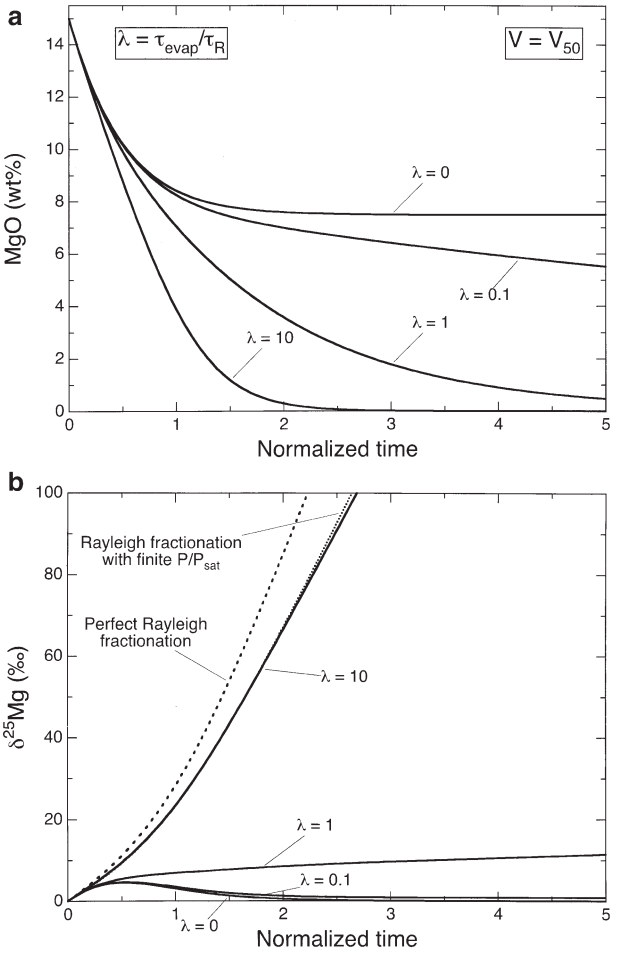

Fig. 16. (a) Same as $V = V_{50}$ case in Figure 15a except that now the volume V need not be closed. The parameter λ measures of the rate of loss of magnesium from V in terms of the evaporation timescale τ_{evap} divided by the residence time τ_R of magnesium in the surrounding gas. $\lambda = 0$ (i.e., very long residence time) corresponds to the closed system case in Figure 15a. (b) Evolution of the magnesium isotopic composition for the four cases shown in panel (a). Also shown are curves for the isotopic evolution corresponding to perfect Rayleigh fractionation (i.e., for $\alpha = (24/25)^{1/2}$ in Eqn. 11) in the free evaporation limit ($\lambda \rightarrow \infty$) and for an effective α' taking into account the finite $P_{Mg}/P_{Mg,sat}$ of the $\lambda = 10$ case (i.e., using α' from Eqn. 52 in Eqn. 11).

of finite $P_i/P_{i,sat}$ on the isotopic fractionation of the residue, which will still follow a Rayleigh fractionation curve but with an effective kinetic isotope fractionation factor α' given by

$$\alpha' - 1 = (\alpha - 1)\left(1 - \frac{P_1}{P_{1,sat}}\right) + \left(\frac{D_1^{gas}}{D_2^{gas}} - 1\right)\frac{P_1}{P_{1,sat}} \quad (52)$$

where $\alpha = \sqrt{m_2/m_1}$. The second term on the right hand side takes into account isotopic fractionation by diffusion through the surrounding gas.

Increasing the hydrogen pressure has two opposite effects on the net evaporation rate. On the one hand, as shown in Figure 4, the free evaporation rate of Mg in the hydrogen-dominated regime increases with hydrogen pressure in proportion to $\sqrt{P_{H_2}}$. Increasing hydrogen pressure will also reduce the net evaporation rate by making it harder for the evaporating species to diffuse away from the surface (i.e., by decreasing D_i^{gas} in Eqn. 51. Figure 17a shows the effect of hydrogen pressure on the net evaporation rate of magnesium from a Type B CAI-like liquid for three choices of the radius of the condensed phase. Figure 17b shows the effect of hydrogen pressure on the isotopic fractionation of magnesium in terms the isotopic fractionation of Mg in a residue from which 50% of the magnesium has evaporated. These results show that for typical chondrule or CAI sizes, the effect of surrounding pressure in reducing the evaporation rate and isotopic fractionation begins to be felt at $\sim 10^{-3}$ bars, and has significant effects at pressures below $\sim 10^{-1}$ bars.

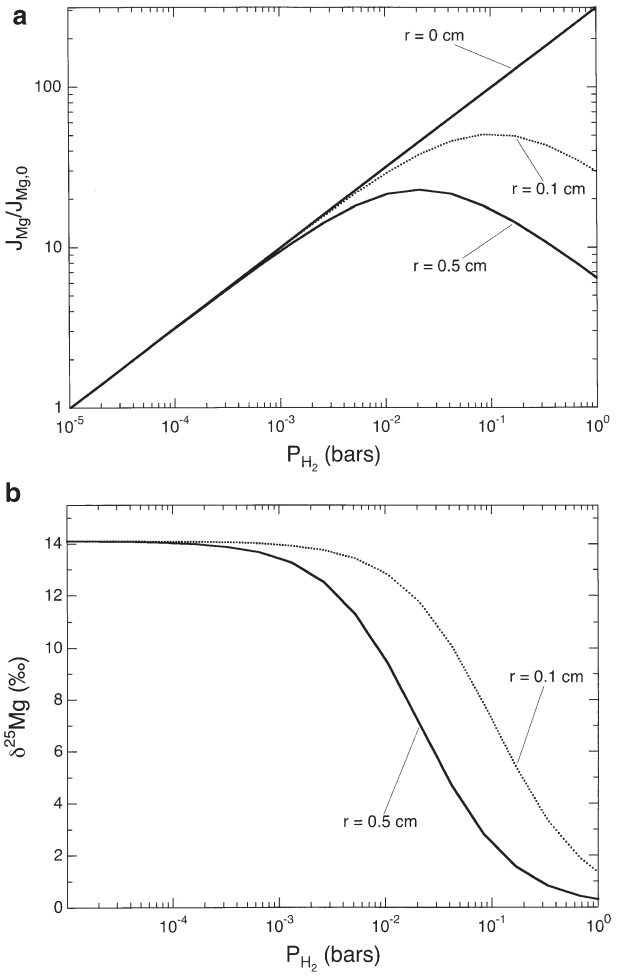

Fig. 17. (a) Effect of hydrogen pressure on the evaporation rate of magnesium (normalized to the rate at $P_{H_2} = 10^{-5}$ bars) illustrated for spheres of radius $r = 0$, 0.1 cm (chondrule-like), and 0.5 cm (CAI-like). In the absence of recondensation ($r = 0$ case), hydrogen, through its effect on the saturation vapor pressure of magnesium, increases the evaporation rate in proportion to $\sqrt{P_{H_2}}$. At sufficiently high surrounding pressure, the diffusion of the evaporating species away from the surface requires that it have a finite partial pressure at the surface, which in turn produces recondensation (see Eqn. 1). This recondensation is responsible for the departure of the magnesium evaporation rate for $r = 0.1$ and 0.5 cm from continuing to increase as $\sqrt{P_{H_2}}$. (b) Effect of hydrogen pressure on the isotopic fractionation of magnesium in evaporation residues illustrated by curves of the fractionation corresponding to 50% loss of magnesium by evaporation from sphere with initial radius of 0.1 and 0.5 cm. The diminished isotopic fractionation at sufficiently high surrounding gas pressure is due to the effect of $P_{Mg}/P_{Mg,sat}$ on the effective kinetic isotope fractionation factor as given by Eqn. 52.

7. SUMMARY AND DISCUSSION

This closing section is used to briefly restate some of the key ideas and conclusions derived from the model problems that show the effect of various timescales on the elemental and isotopic fractionation of condensed phases during evaporation and condensation. The model results are then used to interpret the properties laboratory produced evaporation residues and also to reconsider some of the implications of the volatility-related fractionations of planetary and meteoritic materials.

Given the focus on evaporation and/or condensation, it is most natural to measure time in terms of how long it would take to completely evaporate or condense an element of interest under the prevailing conditions of temperature, pressure, composition and dimensions of the system. Estimates of this timescale as a function of temperature for various choices of pressure and size of the condensed phase were given in Figure 5 for magnesium in a CMAS liquid and in Figure 6 for forsterite. For temperatures in the range where CMAS compositions are partially molten or forsterite is partially condensed from a solar composition gas, the evaporation/condensation timescales are of order days to years. The central set of issues addressed via the model calculations are the consequences for elemental and isotopic fractionation when some of the other timescales affecting evaporation and condensation are fast or slow compared to the evaporation or condensation timescale. The timescales that were explicitly considered involved the rate of change of temperature, the rate of chemical homogenization of the condensed phase by diffusion, and the rate at which evaporated species were removed from further interaction with the condensed phase. Table 1 gives a summary of the consequences of these timescales being large or small compared to the evaporation or condensation timescale.

Some of the timescales listed in Table 1 have had a role in determining the outcome of laboratory evaporation experiments. Vacuum evaporation experiments such as those pioneered by Hashimoto (1983) are designed to be in the regime $P_i/P_{i,sat} \ll 1$, which will be the case when the gas species are rapidly removed from the system (i.e., $\tau_R \ll \tau_{evap}$). In this limit, the isotopic fractionation of the residue is expected to follow a Rayleigh fractionation curve. The magnesium isotope data

Table 1. Timescales for condensation and evaporation.[a]

Timescale	Fractionations	Comments
	Homogeneous phases in closed system (see Fig. 7 and 9)	
$\tau_{cond}/\tau_T < 0.001$	Elemental fractionation *NO* isotopic fractionation during partial condensation	Equilibrium limit
$\tau_{cond}/\tau_T > 0.001$	Elemental and isotopic fractionation during partial condensation	Light-isotope enriched condensate
$\tau_{evap}/\tau_T < 1$ (slow cooling after rapid reheating)	Elemental and isotopic fractionation during partial evaporation	Rayleigh fractionation with heavy-isotope enriched residue
$\tau_{evap}/\tau_T > 1$ (fast cooling after rapid reheating)	Very little elemental and isotopic fractionation	Cooling too fast for significant losses of volatile species by evaporation
	Diffusion-limited systems (see Figs. 10, 11, 12 and 14)	
$\tau_D/\tau_{cond} \gg 1$	Zoned condensates	See Figure 10
$E = \tau_D/\tau_{evap} \gg 100$ (*congruent evaporation*)	No significant isotopic fractionation	Isotopic fractionation restricted to a thin boundary layer (Fig. 11)
$E = \tau_D/\tau_{evap} \gg 100$ (*multi-component evaporation*)	Elemental fractionation No significant isotopic fractionation unless by diffusion in melt	τ_{evap} increases with time due to decreasing concentration of the evaporating species at the surface until $\tau_{evap} \approx \tau_{Diff}$ (Figs. 12, 14)
$\tau_D/\tau_{evap} < 1$ $\tau_D/\tau_{cond} < 1$		Homogeneous condensed phase
	Partially open systems (see Figs. 15 and 16)	
$\tau_{cond}/\tau_R \ll 1$ $\tau_{evap}/\tau_R \ll 1$		Closed system limit (Fig. 15)
$\tau_{cond}/\tau_R \gg 1$	Negligible condensation	Insufficient time to condense
$\tau_{evap}/\tau_R < 0.1$	Elemental fractionation with little or no isotopic fractionation	Elemental fractionation due to the slow removal of an equilibrium gas phase (Fig. 16)
$\tau_{evap}/\tau_R > 10$	Elemental and isotopic fractionation during partial evaporation	Rayleigh fractionation approaching the vacuum evaporation limit (Fig. 16)

[a] τ_{cond} and τ_{evap} are the characteristic timescales for the condensation and evaporation based on the time it would take to condense or evaporate all of the species of interest under the prevailing condition. τ_T is the timesacle of temperature change ($\tau_T = T^{-1}$ dT/dt). τ_D is the diffusive homogenization timescale ($\tau_D = L^2/D$; L is a measure of size, D is the chemical diffusion coefficient). $E = \tau_{evap}/\tau_D$ is the evaporation number defined more specifically in the text. τ_R is a residence timescale of the evaporating species in the gas ($\tau_R = 1/\lambda$ where λ is the fraction of the species removed per unit time by processes other than recondensation).

from vacuum evaporation residues shown in Figure 2 confirms the Rayleigh behavior, however in the case of Mg, the kinetic fractionation factor α is not exactly the expected value of $\sqrt{24/25}$. The reduced isotope fractionation found in the experiments could be explained by recondensation due to $\tau_{evap}/\tau_R <$ 10 (see Fig. 16b), although this does not seem likely because the samples used to construct Figure 2 were of very different sizes ranging from 6 mm to 1 mm in diameter (i.e., very different τ_{evap} but same τ_R) and yet they all have isotopic fractionations falling on a single fractionation line. The evaporation residues were found to be homogeneous in both elemental and isotopic composition, which rules out diffusion-limited evaporation as the cause of $\alpha \neq \sqrt{24/25}$. The most likely explanation of why the experimentally determined α for Mg evaporating from a molten silicate liquid is greater than $\sqrt{24/25}$ is that ^{24}Mg and ^{25}Mg have slightly different sticking coefficients (i.e., $\alpha = (\gamma_{^{25}Mg}/\gamma_{^{24}Mg})\sqrt{24/25}$ and $\gamma_{^{25}Mg}/\gamma_{^{24}Mg} =$ 1.007). Richter et al. (2002b) carried out several experiments in which CMAS liquids were evaporated in one bar of hydrogen slowly flowing through a gas-mixing furnace. The residues had large volatility controlled elemental depletions (up to 60% loss of magnesium relative to aluminum) without any measurable isotopic fractionation of the magnesium in the residues. The lack of magnesium isotopic fractionation despite the large loss of magnesium can be understood in terms of the 1 bar experiments being in a parameter range such that $\tau_{evap}/\tau_R \ll 1$ (i.e., long residence time of the evaporated species in the vicinity of the sample). Figure 16b shows that large elemental fractionations without significant isotopic fractionation would be expected for $\lambda\tau_{evap} < 0.1$. The volume of the gas-mixing furnace is sufficiently small (i.e., $V \ll V_{50}$) that a negligible amount of the magnesium from the condensed phase is sufficient to saturate the gas. Nevertheless, the slow but continuous flow of saturated gas out of the furnace will, given sufficient time, show up as a depletion of the more volatile species from the condensed phase. The 1 bar experiments are a clear example of how elements can be volatilized without leaving behind isotopically fractionated residues. The model calculations not only help us understand the lack of isotopic fractionation of the 1 bar evaporation residues, but also to define the general conditions for such a result to arise.

Isotope fractionations of residues from experiments in which potassium was evaporated from a silicate melt both in air ($P = 10^{-5}$–1 atm) and in hydrogen ($P = 1.3 \times 10^{-2}$–7.2×10^{-5} atm) have been reported by Yu et al. (2003). The reported potassium isotope fractionations (see their fig. 9) as a function of

potassium lost from the melt are very different depending on the pressure of the experiment. Evaporations in 10^{-5} atm of air produced residues with isotopic fractionations of potassium that follow a Rayleigh fractionation curve with a fractionation factor for $^{41}K/^{39}K$ very close to $\alpha = \sqrt{39/41}$. Experiments run at all pressures greater than 10^{-5} atm (even for $P = 1.8 \times 10^{-5}$ atm air) produced isotopic fractionations such that the residues as a function of potassium loss first became heavier (as expected) but then with further loss of potassium, became increasingly light. The results are in some ways quite similar to the closed system results shown in Figure 15b, however it is not at all clear why a furnace tube that is continuously pumped to maintain low pressure should behave as a closed system or why increasing the pressure seems to have the same effect as decreasing the volume of the closed system. The authors suggest that some of the earliest evaporated potassium (and thus isotopically lightest) may have plated out in cooler parts of the furnace and later exchanged potassium with the residue to make the residue isotopically lighter again. No attempt was made to model such a system.

Experiments in the diffusion-limited regime have been carried out for congruently evaporating systems by Wang (1995) and Wang et al. (1999) using solid forsterite, and by Young et al. (1998) using solid SiO_2. Wang (1995) and Wang et al. (1999) showed that the magnesium isotopic fractionations in the solid forsterite decay towards the interior in the manner shown in Figure 11. The evaporation residues from molten CMAS experiments reported by Richter et al. (2002b) and the new samples used to construct Figures 1 and 2 were quenched sufficiently rapidly at the end of the experiments that any chemical or isotopic gradients would have been preserved. No such gradients were observed, which is in good agreement with the expectation that $\tau_D \ll \tau_{evap}$ based on the sample size, the evaporation rate, and the chemical diffusion coefficients in CMAS liquids (see Richter et al., 2002a for magnesium and silicon diffusion coefficients in Type B CAI-like liquids). The lack of chemical or isotopic gradients in the materials used to construct Figure 3 rules out diffusion-limited evaporation as the explanation for the magnesium isotopic fractionations shown in Figure 2 falling below the fractionation expected for $\alpha = \sqrt{24/25}$.

To my knowledge there are no well-controlled experiments directly relevant to the question of kinetic isotope fractionation by condensation. Esat (1988) measured the magnesium isotopic composition of condensates from a gas derived from the distillation of a molten pyroxene source in a bell-jar vacuum chamber ($P = 5 \times 10^{-5}$ torr) and found that the source became enriched in the heavy isotopes of magnesium, while the condensate was enriched in the light isotopes. I would interpret the isotopic fractionations observed by Esat (1988) as being the result of a kinetic fractionation of the source and equilibrium condensation from the gas onto cold surfaces. The source became kinetically fractionated (heavy isotope enriched) because it is evaporating into a low-pressure region from which the evaporating species are rapidly removed by condensation onto cold surfaces (i.e., evaporation with $\tau_{evap}/\tau_R \gg 1$). The magnesium entering the gas is isotopically light and removed almost immediately by condensation onto the cold surfaces, including those that were later analyzed for the magnesium isotopic composition of the condensates. Because the magnesium is for all practical purposes being quantitatively removed from the gas by condensation, the condensate will show the same light isotope enrichment as the gas. Laboratory experiments, that in principle at least, are more directly relevant for determining kinetic isotope fractionations during condensation were carried out by Uyeda et al. (1991). They allowed a low-pressure silicate vapor to condense onto a cold finger whose temperature decreased with distance away from the vapor source. The vapor source and materials condensed at various distances along the cold surface were analyzed for their magnesium isotopic composition. The magnesium isotopic composition of the source was, as expected, somewhat enriched in the heavy isotopes of magnesium. The first (highest temperature) condensate was similarly enriched in the heavy isotopes of magnesium. The authors argued that since the source had become enriched in the heavy isotopes, the evolved gas must have been isotopically light, but since they found the condensate from this gas to be heavy, they were forced to conclude that kinetic condensation produced condensates that were enriched in the heavy isotopes relative to the source gas. This is completely at odds with the theoretical framework adopted in this paper, which predicts that in a kinetic regime the lighter isotopes will condense faster than the heavier ones. Simply put, the results given by Uyeda et al. (1991) cannot be explained by the standard representation of condensation given in Section 2.

The results from the model problems can also be used to identify reasonable parameters that can account for the isotopic properties of solar system materials with volatility related elemental depletion patterns. In the case of the Type B CAIs one would like to find conditions that would result in their magnesium isotopic compositions being enriched in the heavy isotopes by 1–5‰ per amu. Partial melting of Type B–like compositions requires temperatures of ~1700 K (Stolper, 1982) and their coarse-grained textures can be reproduced if the subsequent cooling rates are less than 50 K/h (Stolper and Paque, 1986). The model results shown in Figures 9a,b provide an alternative way of constraining the cooling rate based on the evaporation kinetic and associated isotopic fractionation. The requirement that some magnesium remain when the Type B CAIs become completely solid again at T ~ 1400 K implies $\tau_{evap}/\tau_T > 0.03$. A more stringent requirement comes from the magnesium isotopic composition, which will be fractionated by 1–5‰ per amu if $0.3 < \tau_{evap}/\tau_T < 1$. Taking numerical values for τ_{evap} from Figure 5 and keeping in mind that τ_T was defined in terms of the timescale for the temperature to drop by a factor of e (~500 K), the cooling rates that are consistent with 1–5‰ per amu magnesium isotopic fractionation of a 2.5 mm radius Type B CAI are $dT/dt \approx 25$ K h^{-1} if evaporation takes place in 10^{-3} bars of hydrogen, and $dT/dt \approx 1$ K h^{-1} in 10^{-6} bars of hydrogen. These estimates of the cooling rate of Type B CAIs with magnesium isotope fractionations of the order of 1–5‰ per amu are very similar to the values given in Figure 15 of Richter et al. (2002b) based on much more detailed calculations. The merit of deriving cooling rate estimates from simple arguments based on relative timescales is that it makes it that much easier to understand how the properties of the CAIs and the environment combine to determine the degree of isotopic fractionation of evaporation residues.

Chondrules often also have textures that suggest that they were reheated and partially molten, and yet, the isotopic com-

position of the relatively volatile element potassium is not measurably fractionated. One possible explanation for this is that the cooling must have been sufficiently fast so that little or no potassium evaporated. If that were true, then the differences in the relative abundance of potassium as reflected by K/Al ratios would then have to have been due to some process other than volatilization. Using Figure 9a as a guide, little measurable isotopic fractionation would be expected if $\tau_{evap}/\tau_T > 1$. The evaporation time for potassium for a chondrule of radius 500 μm and 1 wt % K_2O can be estimated using the evaporation kinetics reported by Yu et al. (2003), $J_K \approx 1 \times 10^{-7}$ moles cm^{-2} s^{-1} for $T \approx 1750$ K, giving $\tau_{evap} \approx 1$ min. It follows that $\tau_{evap}/\tau_T > 1$ implies that the cooling rate would have to have been greater than 3×10^4 K h^{-1}. This bound on the cooling rate is similar to that estimated by Alexander et al. (2000) as being necessary to prevent more than 12% K loss from a 1 mm diameter chondrule heated to a peak temperature in the range 1700–1800 K. A cooling rate of 3×10^4 K h^{-1} is one to four orders of magnitude faster than the laboratory cooling rates that have been used to reproduce chondrule textures (see tables 1 and 2 in Desch and Connolly, 2002 for a summary). Alexander et al. (2000) are quite right in pointing out that if one accepts the laboratory cooling rates as reasonable estimates of the actual cooling rate of chondrules, the issue becomes one of finding conditions that would suppress potassium isotope fractionation at these "slow" (i.e., $\tau_{evap}/\tau_T < 1$) cooling rates. Their suggestion is that evaporation of potassium from fine-grained dust and chondrule precursors during chondrule formation may have produced sufficient potassium vapor pressure for gas-chondrule isotopic exchange to be complete on the timescales of chondrule formation. The model problems described in Section 6 can give some insight as to what would be required for this suggestion to be effective. It follows from the results shown in Figures 15 and 16 that to suppress isotopic fractionation of the residues the system would have to be in the parameter range $\tau_{evap}/\tau_R < 0.1$ (i.e., long residence time for the evaporating species in the surrounding gas). The isotopic equilibration takes place on a timescale of a few evaporation times τ_{evap}, which is short compared to the cooling times inferred from the laboratory experiments. Based on the results given in Figure 15a, one should add the requirement that the volume density of chondrules has to be sufficiently high for the gas to become saturated before the potassium is completely volatilized. In the terms used in Section 6, this means that the volume V per chondrule should not be much greater than 10 times the volume that would be saturated by half the potassium originally in the chondrule (i.e., V not much larger than $10V_{50}$). The volume density of chondrules is a particularly interesting parameter in that chondrules reheated in environments with different amounts of chondrules per unit volume (i.e., different V/V_{50}) would end up with different degrees of potassium depletion (as for the various cases in Fig. 15a, but for potassium instead of magnesium) but with little or no associated potassium isotopic fractionation.

Another regime that has been invoked to explain volatile-element depletions with little or no associated isotopic fractionation is diffusion-limited evaporation. Young (2000), for example, used a high Peclet number evaporation model (i.e., fast evaporation relative to diffusion) to discuss the lack of potassium isotope variation between solar system materials with very different degrees of potassium depletion relative to the more refractory elements. Galy et al. (2000) suggested that evaporation with high Peclet number might explain why they measured very little fractionation of magnesium isotopes in chondrules that varied in Mg/Al by more than an order of magnitude. It should be noted that the evaporation model used by Young (2000) and by Galy et al. (2000) is the same one-component evaporation model that was first used by Young et al. (1998) in their discussion of diffusion-limited evaporation of SiO_2. This is a congruent evaporation model and therefore cannot be used to discuss the relationship between elemental and isotopic fractionation in a multi-component system because by definition there is no elemental fractionation in a congruent evaporation model. In terms of the potassium and magnesium isotopic data that Young (2000) and Galy et al. (2000) were trying to explain, the key question is whether a diffusion-limited multicomponent system can loose a significant amount of its more volatile components without a measurable associated isotopic fractionation of the residue. The answer, based on the model results given in Section 5.3, is very likely to be no, because of isotopic fractionation associated with the diffusive transport of material from the interior of the condensed phase to the evaporating surface. Fractionation of magnesium and potassium isotopes by diffusion in silicate melts have not yet been measured, but given the Richter et al. (2003) demonstration of diffusive fractionations of calcium and lithium isotopes by diffusion in silicate melts, it seems reasonable to expect that magnesium and potassium isotopes will be similarly fractionated.

Humayun and Clayton (1995), as noted in the introduction, interpreted their potassium isotopic measurements as indicating that partial condensation was the dominant process responsible for the volatile depletion patterns of solar system materials and that no more than 2% of the potassium could have been removed by partial volatilization from the samples they analyzed. I would interpret the lack of potassium isotope variability of solar system materials quite differently. A sufficient condition for elemental fractionation without isotopic fractionation by either partial evaporation or partial condensation is that $P_i/P_{i,sat}$ remain very close to one as the system evolves, and this condition would be expected whenever the timescale on which the temperature evolves is slow compared to the evaporation or condensation timescale. Given that the large-scale thermal evolution of the early solar system from a gas and dust cloud to the point of producing solids we might sample today was on a timescale of 10^5 yr or more, it seems very likely that large-scale chemical processes involving exchange between gas and condensed phases would have taken place in condition indistinguishable from equilibrium (i.e., $\tau_T \gg \tau_{cond}$ or τ_{evap}). Under this interpretation the lack of potassium isotopic fractionation tells us nothing about the relative importance of condensation and evaporation.

A number of the issues associated with kinetic isotope fractionation by evaporation discussed here in terms of simple model problems have also been addressed in several recent papers using far more detailed models in more specific contexts. For example, the effect of recondensation on elemental and isotopic fractionation has been discussed by several authors including Tsuchiyama et al. (1999), Humayun and Cassen (2000), Ozawa and Nagahara (2001), Richter et al. (2002b),

and most recently by Grossman and Fedkin (2003). All of these papers recognized that the key parameter governing recondensation is $P_i/P_{i,sat}$, which follows directly from Eqn. 1, and come to similar conclusions as to how isotope fractionation is affected by finite $P_i/P_{i,sat}$. What distinguishes the present approach is that the models have been idealized and simplified to allow one to more easily recognize how the various timescales of the evaporation problem determine the magnitude of $P_i / P_{i,sat}$ and the associated departures of the isotopic fractionations from perfect Rayleigh fractionation. Simple models can also make certain potentially puzzling results easier to understand by stripping the problem down to its most essential aspects. An example of this is seen in the discussion of the diffusion-limited evaporation of a multicomponent system where the elemental fractionation can extend throughout the sample but the isotopic fractionations are restricted to a boundary layer. Ozawa and Nagahara (2001) have also shown model results in which the elemental and isotopic fractionations occur over very different length scales but they did not discuss this curious result in any detail and they did not consider how isotope fractionation by diffusion might modify the results. In the most general sense, the role of idealized models is to enhance our intuition regarding the systems of interest by providing natural measures of fast vs. slow; big vs. small. Developing an intuitive grasp of the conditions that allow evaporating and/or condensing systems to fractionate elements with or without associated isotopic fractionation is an essential step towards being able to exercise independent critical judgment regarding specific claims as to the role that evaporation and condensation played in establishing the diverse chemical properties of solar system materials.

Acknowledgments—I am extremely fortunate and grateful for all the help and advice I get from Andy Davis. Much of this manuscript was prepared while I was on sabbatical leave at the Field Museum collaborating with Meenakshi Wadhwa and Philip Janney. The final version of this paper is significantly improved from the original thanks to detailed reviews by Hiroko Nagahara and Shogo Tashibana. The research reported here was supported by NASA Grant NAG5-13027.

Associate editor: A. N. Krot

REFERENCES

Alexander C. M. O'D., Grossman J. N., Wang J., Zanda B., Bourot-Denise M., and Hewins R. H. (2000) The lack of potassium-isotope fractionation in Bishunpur chondrules *Meteoritcs* **35,** 859–868.

Alexander C. M. O'D. and Wang J. (2001) Iron isotopes in chondrules: Implications for the role of evaporation during chondrule formation. *Meteoritcs* **36,** 419–428.

Berman R. G. (1983) A thermodynamic model for multicomponent melts, with application to the system CaO-MgO-Al_2O_3-SiO_2, Ph.D. dissertation. University of British Columbia.

Carslaw H. S. and Jaeger J. C. (1959) *Conduction of Heat in Solids.* Clarendon Press.

Clayton R. N., Hinton R. W., and Davis A. M. (1988) Isotopic variations in the rock-forming elements in meteorites. *Philos. Trans. R. Soc. Lond. A* **325,** 483–501.

Davis A. M., Hashimoto A., Clayton R. N., and Mayeda T. K. (1990) Isotope mass fractionation during evaporation of forsterite (Mg_2SiO_4). *Nature* **347,** 655–658.

Desch S. J. and Connolly H. C. Jr. (2002) A model of the thermal processing of particles in solar nebula shocks: Applications to the cooling rate of chondrules. *Meteoritics* **37,** 183–202.

Ebel D. S. and Grossman L. (2000) Condensation in dust-enriched systems. *Geochim. Cosmochim. Acta* **64,** 339–366.

Esat T. M. (1988) Physicochemical isotope anomalies. *Geochim. Cosmochim. Acta* **52,** 1409–1424.

Galy A., Young E. D., Ash R. D., and O'Nions R. K. (2000) the formation of chondrules at high gas pressures in the solar nebula. *Science* **290,** 1751–1753.

Grossman L. (1972) Condensation in the primitive solar nebula. *Geochim. Cosmochim. Acta* **36,** 597–619.

Grossman L., Ebel D. S., Simon S. B., Davis A. M., Richter F. M., and Parsad N. M. (2000) Major element chemical and isotopic compositions of refractory inclusions in C3 chondrites: The separate roles of condensation and evaporation. *Geochim. Cosmochim. Acta* **64,** 2879–2894.

Grossman L., Ebel D. S., and Simon S. B. (2002) Formation of refractory inclusions by evaporation of condensate precursors. *Geochim. Cosmochim. Acta* **66,** 145–161.

Grossman L. and Fedkin A. V. (2003) CaO-MgO-Al_2O_3-SiO_2 liquids: Chemical and isotopic effects of Mg and Si evaporation in a closed system of solar composition. *Geochim. Cosmochim. Acta* **67,** 4205–4221.

Hashimoto A. (1983) Evaporation metamorphism in the early solar nebula—Evaporation experiments on the melt FeO-MgO-SiO_2-CaO-Al_2O_3 and chemical fractionations of primitive materials. *Geochem. J.* **17,** 111–145.

Hinton R. W., Clayton R. N., Olsen E. J., and Davis A. M. (1987) Isotopic mass fractionation of potassium in the Earth compared to the bulk solar system. *Lunar Planet. Sci.* **18,** 429–430.

Hinton R. W., Clayton R. N., Davis A. M., and Olsen E. J. (1988) Isotopic mass fractionation of potassium in the Moon. *Lunar Planet. Sci.* **19,** 497–498.

Hirth J. P. and Pound G. M. (1963) *Condensation and Evaporation Nucleation and Growth Kinetics.* Pergamon Press.

Humayun M. (2001) Comment on "Assessing the implications of K isotope geochemistry for evaporation in the preplanetary solar nebula" by E. Young. *Earth Planet. Sci. Lett.* **192,** 93–99.

Humayun M. and Clayton R. N. (1995) Potassium isotope cosmochemistry: Genetic implications of volatile element depletion. *Geochim. Cosmochim. Acta* **59,** 2131–2148.

Humayun M. and Cassen P. (2000) Processes determining the volatile abundances of the meteorites and terrestrial planets. In *Origin of the Earth and Moon* (eds. R. M. Canup and K. Righter). University of Arizona Press. 3–23.

Janney P. E., Davis A. M., Wadhwa M., Mendybaev R. A., and Richter F. M. (2003) High precision magnesium isotopic measurements of CAI evaporation residues. *Lunar Planet. Sci.* **34,** 1940.

Kuroda D. and Hashimoto A. (2002) The reaction of forsterite with hydrogen—Its apparent and real temperature dependences. *Antarctic Meteor. Res.* **15,** 152–164.

Larimer J. W. (1967) Chemical fractionations in meteorites—I. Condensation of the elements. *Geochim. Cosmochim. Acta* **31,** 1215–1238.

Lofgren G. E. and Lanier A. B. (1990) Dynamic recrystallization study of barred olivine chondrules. *Geochim. Cosmochim. Acta* **54,** 3537–3551.

McDonough W. F. and Sun S. S. (1995) The composition of the Earth. *Chem. Geol.* **120,** 223–253.

Mendybaev R. A., Richter F. M., and Davis A. M. (2003) Formation of the melilite mantle of the Type B CAIs: Experimental simulations. *Lunar Planet. Sci.* **34,** 2062.pdf.

Ozawa K. and Nagahara H. (2001) Chemical and isotopic fractionation by evaporation and their cosmochemical implications. *Geochim. Cosmochim. Acta* **65,** 2171–2199.

Palme H. and Boynton W. V. (1993) Meteoritic constraints on conditions in the solar nebula. In *Protostars and Planets 3* (eds. E. H. Levy and J. I. Lunine), pp. 979–1004. University of Arizona Press.

Radomsky P. M. and Hewins R. H. (1990) Formation conditions of pyroxene-olivine and magnesian olivine chondrules. *Geochim. Cosmochim. Acta* **54,** 3475–3490.

Rayleigh J. W. S. (1896) Theoretical considerations respecting the separation of gases by diffusion and similar processes. *Philos. Mag.,* 5th ser., **42,** 493–498.

Richter F. M., Liang Y., and Davis A. M. (1999) Isotope fractionation by diffusion in molten oxides. *Geochim. Cosmochim. Acta* **63,** 2853–2861.

Richter F. M., Davis A. M., and Mendybaev R. A. (2002a) How the B1s got their melilite mantles. *Lunar Planet. Sci.* **33,** 1901.pdf.

Richter F. M., Davis A. M., Ebel D. S., and Hashimoto A. (2002b) Elemental and isotopic fractionation of Type B calcium-, aluminum-rich inclusions: Experiments, theoretical considerations and constraints on their thermal evolution. *Geochim. Cosmochim. Acta* **66,** 521–540.

Richter F. M., Davis A. M., DePaolo D. J., and Watson E. B. (2003) Isotope fractionation by chemical diffusion between molten basalt and rhyolite. *Geochim. Cosmochim. Acta* **67,** 3905–3923.

Stolper E. (1982) Crystallization sequences of calcium-aluminum–rich inclusions from Allende: An experimental study. *Geochim. Cosmochim. Acta* **46,** 2159–2180.

Stolper E. and Paque J. M. (1986) Crystallization sequences of calcium-aluminum-rich inclusions from Allende: The effects of cooling rate and maximum temperature. *Geochim. Cosmochim. Acta* **50,** 1785–1806.

Taylor S. R. (1992) *Solar System Evolution: A New Perspective.* Cambridge University Press.

Tsuchiyama A., Kawamura K., Nakao T., and Uyeda C. (1994) Isotopic effects on diffusion in MgO simulated by molecular dynamics: Method and implications for isotopic mass fractionation in magmatic systems. *Geochim. Cosmochim. Acta* **58,** 3013–3021.

Tsuchiyama A., Tachibana S., and Takahashi T. (1999) Evaporation of forsterite in the primordial solar nebula: Rates and accompanied isotopic fractionation. *Geochim. Cosmochim. Acta* **63,** 2451–2466.

Uyeda C., Tsuchiyama A., and Okano J. (1991) Magnesium isotope fractionation of silicates produced in condensation experiments. *Earth Planet. Sci. Lett.* **107,** 138–147.

Wang J. (1995) Chemical and isotopic fractionation during the evaporation of synthetic forsterite and material of solar composition. Ph.D. dissertation. University of Chicago.

Wang J., Davis A. M., Clayton R. N., Mayeda T. K. (1994) Kinetic isotope fractionation during the evaporation of the iron oxide from the liquid state. *Lunar Planet. Sci.* **25,** 1457–1458.

Wang J., Davis A. M., Clayton R. N., and Hashimoto A. (1999) Evaporation of single crystal forsterite: Evaporation kinetics, magnesium isotope fractionation and implications of mass-dependent isotopic fractionation of a diffusion-controlled reservoir. *Geochim. Cosmochim. Acta* **63,** 953–966.

Wang J., Davis A. M., Clayton R. N., Mayeda T. K., and Hashimoto A. (2001) Chemical and isotopic fractionation during the evaporation of the FeO-MgO-SiO_2-CaO-Al_2O_3-TiO_2-REE melt system. *Geochim. Cosmochim. Acta* **65,** 479–494.

Wänke H. and Dreibus G. (1988) Chemical composition and accretion history of terrestrial planets. *Phil. Trans. Roy. Soc. Lond. A* **325,** 545–557.

Yoneda S. and Grossman L. (1995) Condensation of CaO-MgO-Al_2O_3-SiO_2 liquids from cosmic gases. *Geochim. Cosmochim. Acta* **59,** 3413–44.

Young E. D. (2000) Assessing the implications of K isotope geochemistry for evaporation in the preplanetary solar nebula. *Earth Planet. Sci. Lett.* **183,** 321–333.

Young E. D., Nagahara H., Mysen B. O., and Audet D. M. (1998) Non-Rayleigh oxygen isotope fractionation by mineral evaporation: Theory and experiments in the system SiO_2. *Geochim. Cosmochim. Acta* **62,** 3109–3116.

Yu Y., Hewins R. H., Alexander C. M. O'D., and Wang J. (2003) Experimental study of evaporation and isotopic mass fractionation of potassium in silicate melts. *Geochim. Cosmochim. Acta* **67,** 773–786.